TABLE 3 Correlation of CGS and IGS results between NB and RP specimens

	RP GS, *n*		
NB	≤6	7	8–10
CGS			
NB GS			
≤6	26	20	2
7	3	27	7
8–10	0	5	13
IGS			
NB GS	23	18	1
≤6			
7	3	29	9
8–10	0	0	20

TABLE 4 Comparison of CGS and IGS of NB and RP specimens

	IGS, *n*			
CGS	≤6	7	8–10	Total
NB*				
CGS				
≤6	34	14	0	48
7	8	22	7	37
8–10	0	5	13	18
Total	42	41	20	103
RP†				
CGS				
≤6	18	11	0	29
7	8	34	10	52
8–10	0	2	20	22
Total	26	47	30	103

*Mann–Whitney U-test, P = *0.469, †0.329.*

with that of the RP specimen in 66 cases (64%). The under-grading rate was 28% (29 cases) and the over-grading rate was 8% (eight cases) for CGS. IGS yielded an under-grading rate of 27% (28 cases), similar to the CGS results. The concordance rate for IGS was slightly higher (70%) than that for CGS, while the over-grading rate was significantly lower with IGS (3%, three cases) than with CGS (8%, eight cases; $P = 0.026$).

Next, we compared the CGS and IGS of NB and RP specimens (Table 4). Although the concordance rates for NB and RP specimens by CGS and IGS were similar, at 67% and 70%, the IGS were higher, by 16% in NB and by 20% in RP specimens, than CGS. However, there were no significant differences between

Risk	IGS, *n*			
classification	Low	Intermediate	High	Total
CGS				
Low	24	10	0	34
Intermediate	5	28	4	37
High	0	4	28	32
Total	29	42	32	103

TABLE 5 Risk classifications with CGS and IGS

Mann–Whitney U-test, P = 0.678.

	Pathological stage				
NB GS	pT2	pTa	pTb	Total	P chi-square
CGS					0.198
≤6	37	10	1	48	
≥7	26	19	6	51	
IGS					
≤6	30	9	0	39	
≥7	33	20	7	60	

TABLE 6 Comparison of NB GS and pathological staging of RP specimens

FIG. 1. Associations of BRFS according to GS from NB specimens graded by CGS and IGS. (a) In three groups, i.e. CGS ≤6, 7 and ≥8, BFRS was evaluated after RP. (b) In three groups, i.e. IGS ≤6, 7 and ≥8, BFRS was evaluated after RP.

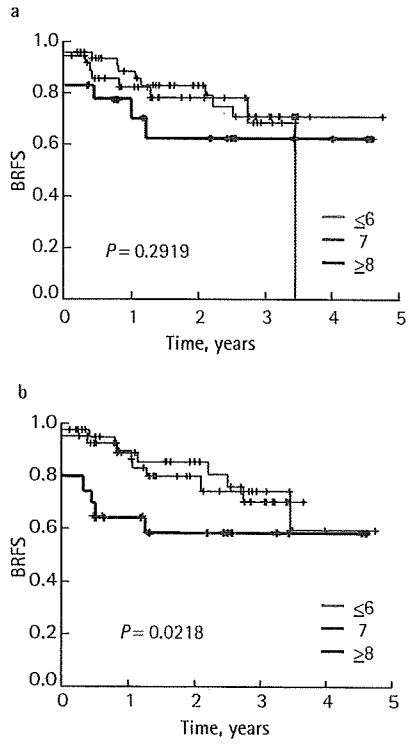

CGS and IGS ($P = 0.469$ for NB and $P = 0.329$ for RP, Mann–Whitney *U*-test). Over-grading rates for NB and RP specimens were 13% and 10% by CGS and IGS, respectively.

Table 5 shows the results grouped by the risk categories of D'Amico *et al.* [9]; 10 (29%) of the 34 categorized as low-risk, based on IGS, were intermediate-risk according to CGS results. Five (14%) and four (11%) of the 37 intermediate-risk, based on CGS, patients were low- and high- risk, respectively, by IGS. However, there were no statistically significant differences in risk classification between CGS and IGS ($P = 0.678$, Mann–Whitney *U*-test).

Clinical staging showed that T1c and T2 each accounted for half the patients; we compared the components of RP pathological staging by CGS and IGS of NB specimens, divided into two groups, GS ≤6 and ≥7. As shown in Table 6, pathological staging by CGS showed predominantly pT2 and pT3a lesions. Among the patients with CGS ≤6 for NB specimens, 37% (pT2) had organ-confined lesions, while 26% of those with CGS ≥7 had organ-confined lesions. However, by contrast with the CGS results, IGS showed an increase in GS ≥7 cases (33%) among those with pT2 tumours, and similar results were obtained for pT3 cases, i.e. 20% in pT3a and 7% in pT3b. However, none of the differences in pathological staging between CGS and IGS were statistically significant ($P = 0.198$, chi-square test).

As shown in Fig. 1A, BRFS in patients with NB specimens classified by CGS did not differ significantly among the three GS groups (≤6, 7 and ≥8). However, when IGS was applied to re-evaluate NB specimens, there was a significant difference in BRFS among these

three groups ($P = 0.022$; Fig. 1B). Likewise, the BRFS in RP specimens, classified by CGS or IGS, were analysed. There were no significant differences in BRFS among the three groups when RP specimens were classified by CGS. However, as when IGS was used to classify NB specimens, the BRFS differed significantly among the three groups ($P = 0.045$; data not shown).

DISCUSSION

The present study showed that nearly a quarter of NB specimens were under-graded in comparison with RP specimens, according to both CGS and IGS evaluations. The GS concordance rates between NB and RP specimens in this study were 64% and 70% by CGS and IGS, respectively, rates similar to those of previous reports (30–74%) [10]. Although we anticipated increased GS up-grading with IGS in both NB and RP specimens, the up-grading rates were only 16% and 20%, respectively. Interestingly, the GS classification of NB by IGS reflected BRFS after RP, although that by CGS did not. Thus, IGS is more reliable for treatment decision-making, especially for early-stage prostate cancer managed with RP, brachytherapy, external beam radiotherapy, hormonal therapy or active surveillance [11].

It was previously reported that the NB pathological findings of focal prostate cancers are not a reliable surrogate indicator, and thus should not influence treatment decisions. One explanation is that prostate cancer is a multifocal disease with satellite tumours [12]. Horinger *et al.* [13] reported that 52 RP specimens had multifocality, showing altogether 196 foci of prostate cancer (the mean number of cancer foci per specimen was 3.76). Other earlier reports also showed that most prostate cancers with high or low tumour volumes were multifocal [14,15]. In these reports, more intriguing results were documented, i.e. very small prostate cancer foci had high GS [13,15]. This might explain why the CGS of NB fails to predict the CGS of RP specimens. CGS does not indicate tertiary cancer lesions or small cancer foci in NB specimens with relatively high Gleason grades, while IGS indicates the primary pattern and the highest grade even in cancer lesions which have small volumes in NB specimens. The present observation that IGS of NB specimens showed significant differences in BRFS after RP suggests the importance of documenting the highest GS in NB.

Khoddami *et al.* [16] reported that primary Gleason pattern 4 had predictive value in patients with Gleason score 7 tumours after RP, meaning that a higher Gleason pattern is important for the prognosis of localized tumours after RP or radiotherapy. From the current results we conclude that the influence of IGS on clinical outcome reflects the grading of NBs based even on minimal findings of high-grade tumour cells. We speculate that Gleason himself might not have recognized the importance of small areas of a third pattern, especially those with the highest grade pattern [17]. However, unlike in the Gleason era, many thin cores from different sites in the prostate can currently be obtained by sextant needle biopsies in patients with early-stage disease, e.g. T1c tumours. Recently, to determine optimum treatments for localized prostate cancer, use of the Partin table, which predicts tumour extension by combining PSA level, clinical stage and GS, has become widespread [18]. Hence, the Partin table might be influenced by IGS, and accumulation of more pathological data on RP specimens will be needed to obtain a new 'Partin table'. Although urologists should prospectively consider differences in NB pathology between CGS or IGS, in practice it would be better to use IGS to obtain of the newest and most reliable nomogram for predicting the outcome of this disease. It is well understood that taking more biopsy cores improves the accuracy of the GS obtained by biopsy in predicting the final GS at RP [9,19]. Furthermore, Antunes *et al.* [20] reported that the percentage of positive biopsy cores reflected the biochemical outcome after RP. In addition, the present results show pathological grading by IGS to reconfirm the accuracy of the biopsy GS before applying treatments for localized prostate cancer.

We showed that 27% more NB than RP specimens were under-graded by IGS, while 28% of NB specimens were under-graded by CGS. The under-grading rate with IGS in our data is consistent with those of earlier reports using CGS [10,21,22]. Previously, GS under-grading of NB specimens was the most prevalent error in comparison with GS grading of RP specimens. Even when the same pathologist assessed both samples, a third of them were still under-graded [22]. Although in the present study the same pathologist evaluated both NB and RP specimens by IGS, the under-grading rate was no less than that by CGS (Table 2). The study of King [23] documented that biases in pathological interpretation and sampling effects contribute to grading discordance. A bias problem in pathological interpretation might be resolved by the widespread use of IGS, especially introducing an assessment of NB specimens.

Fukagai *et al.* [24] indicated that grading errors were most frequent in well-differentiated carcinoma, and that most involved under-grading with poorer NB-RP correlations. They suggested that pathologists tend to under-grade biopsies of moderately differentiated carcinoma as well-differentiated carcinoma. Furthermore, a recent study, examining trends in GS over a period of 15 years, showed that tumours reported as GS ≤6 in NB specimens are prone to be under-graded, while those reported as GS 8–10 are prone to be over-graded [5]. In the light of the change in the GS reporting trend between 1992 and 2006, a progressive increase in Gleason grade 3 and a decrease in Gleason grade 2 were confirmed [25], showing a tendency for an increase in the incidence of moderately differentiated tumours and a decrease in that of well-differentiated tumours. Based on those analyses, the reduction in GS discrepancy between NB and RP specimens would be expected from the redefinition of the Gleason grading system for NB specimens [26,27]. In this respect, the IGS system provides a new definition, described above. The Consensus Conference on Gleason Grading of Prostatic Carcinoma recommended that the GS be the sum of the most common and the highest grade patterns, and that cribriform patterns be diagnosed as Gleason pattern 4 with only rare cribriform lesions satisfying the diagnostic criteria for cribriform pattern 3 [8]. According to the IGS system, under-grading of NB, i.e. GS ≤6, would decrease markedly, while over-grading, i.e. GS >6, would increase.

In conclusion, although the GS under-grading rates in NB and RP specimens did not differ between the CGS and IGS systems, the GS of NB specimens determined by IGS were associated with a significant difference in BRFS after RP, with GS scores similar to those determined using RP specimens. Given that an extended NB scheme and/or the development of a more suitable ultrasound device is expected, the IGS system would

enhance the accuracy of histological assessments of prostate cancer. This will allow physicians caring for patients with prostate cancer to optimize therapies such as RP, brachytherapy, external beam radiotherapy and active surveillance.

ACKNOWLEDGEMENTS

This study was supported by a Grant-in-Aid for Scientific Research (C) from the Ministry of Education, Culture, Science and Technology, a grant for the 2007 Suzuki Foundation, Yamaguchi Endocrine Disease Foundation, the Third-term Cancer Control Strategy Program from the Ministry of Health, Labor and Welfare, and a grant for 2008 Strategic Research Projects (No. K20003 and K20010) of Yokohama City University, Japan.

CONFLICT OF INTEREST

None declared.

REFERENCES

1 **Draisma G, Boer R, Otto SJ *et al.*** Lead times and overdetection due to prostate-specific antigen screening: estimates from the European Randomized Study of Screening for Prostate Cancer. *J Natl Cancer Inst* 2003; **95**: 868–78

2 **D'Amico AV, Whittington R, Malkowicz SB *et al.*** Pretreatment nomogram for prostate-specific antigen recurrence after radical prostatectomy or external-beam radiation therapy for clinically localized prostate cancer. *J Clin Oncol* 1999; **17**: 168–72

3 **Partin AW, Kattan MW, Subong EN *et al.*** Combination of prostate-specific antigen, clinical stage, and Gleason score to predict pathological stage of localized prostate cancer. A multi-institutional update. *JAMA* 1997; **277**: 1445–51

4 **Sved PD, Gomez P, Manoharan M *et al.*** Limitations of biopsy Gleason grade: implications for counseling patients with biopsy Gleason score 6 prostate cancer. *J Urol* 2004; **172**: 98–102

5 **Rajinikanth A, Manoharan M, Soloway CT *et al.*** Trends in Gleason score: concordance between biopsy and prostatectomy over 15 years. *Urology* 2008; **72**: 177–82

6 **Mian BM, Lehr DJ, Moore CK *et al.*** Role of prostate biopsy schemes in accurate prediction of Gleason scores. *Urology* 2006; **67**: 379–83

7 **San Francisco IF, DeWolf WC, Rosen S *et al.*** Extended prostate needle biopsy improves concordance of Gleason grading between prostate needle biopsy and radical prostatectomy. *J Urol* 2003; **169**: 136–40

8 **Epstein JI, Allsbrook WC Jr, Amin MB, Egevad LL.** The 2005 International Society of Urological Pathology (ISUP) Consensus Conference on Gleason Grading of Prostatic Carcinoma. *Am J Surg Pathol* 2005; **29**: 1228–42

9 **D'Amico AV, Whittington R, Malkowicz SB *et al.*** Calculated prostate cancer volume greater than 4.0 cm3 identifies patients with localized prostate cancer who have a poor prognosis following radical prostatectomy or external-beam radiation therapy. *J Clin Oncol* 1998; **16**: 3094–100

10 **Koksal IT, Ozcan F, Kadioglu TC *et al.*** Discrepancy between Gleason scores of biopsy and radical prostatectomy specimens. *Eur Urol* 2000; **37**: 670–4

11 **Hardie C, Parker C, Norman A *et al.*** Early outcomes of active surveillance for localized prostate cancer. *BJU Int* 2005; **95**: 956–60

12 **Donohue RE, Miller GJ.** Adenocarcinoma of the prostate: biopsy to whole mount. The Denver VA experience. *Urol Clin North Am* 1991; **18**: 449–52

13 **Horninger W, Berger AP, Rogatsch H *et al.*** Characteristics of prostate cancers detected at low PSA levels. *Prostate* 2004; **58**: 232–7

14 **Djavan B, Mazal P, Zlotta A *et al.*** Pathological features of prostate cancer detected on initial and repeat prostate biopsy: results of the prospective European Prostate Cancer Detection study. *Prostate* 2001; **47**: 111–7

15 **Djavan B, Susani M, Bursa B *et al.*** Predictability and significance of multifocal prostate cancer in the radical prostatectomy specimen. *Tech Urol* 1999; **5**: 139–42

16 **Khoddami SM, Shariat SF, Lotan Y *et al.*** Predictive value of primary Gleason pattern 4 in patients with Gleason score 7 tumours treated with radical prostatectomy. *BJU Int* 2004; **94**: 42–6

17 **Gleason DF.** Histological grading and clinical staging of prostatic carcinoma. In Tannenbaum M ed., *Urologic Pathology: the Prostate*. Philadelphia: Lea and Feibiger, 1977: 171–98

18 **Richstone L, Bianco FJ, Shah HH *et al.*** Radical prostatectomy in men aged > or = 70 years: effect of age on upgrading, upstaging, and the accuracy of a preoperative nomogram. *BJU Int* 2008; **101**: 541–6

19 **Coogan CL, Latchamsetty KC, Greenfield J *et al.*** Increasing the number of biopsy cores improves the concordance of biopsy Gleason score to prostatectomy Gleason score. *BJU Int* 2005; **96**: 324–7

20 **Antunes AA, Srougi M, Dall'Oglio MF *et al.*** The percentage of positive biopsy cores as a predictor of disease recurrence in patients with prostate cancer treated with radical prostatectomy. *BJU Int* 2005; **96**: 1258–63

21 **Divrik RT, Eroglu A, Sahin A *et al.*** Increasing the number of biopsies increases the concordance of Gleason scores of needle biopsies and prostatectomy specimens. *Urol Oncol* 2007; **25**: 376–82

22 **Lattouf JB, Saad F.** Gleason score on biopsy: is it reliable for predicting the final grade on pathology? *BJU Int* 2002; **90**: 694–8

23 **King CR.** Patterns of prostate cancer biopsy grading: trends and clinical implications. *Int J Cancer* 2000; **90**: 305–11

24 **Fukagai T, Namiki T, Namiki H *et al.*** Discrepancies between Gleason scores of needle biopsy and radical prostatectomy specimens. *Pathol Int* 2001; **51**: 364–70

25 **Sengupta S, Slezak JM, Blute ML *et al.*** Trends in distribution and prognostic significance of Gleason grades on radical retropubic prostatectomy specimens between 1989 and 2001. *Cancer* 2006; **106**: 2630–5

26 **Gleason DF.** Histologic grading of prostate cancer: a perspective. *Hum Pathol* 1992; **23**: 273–9

27 **Epstein JI.** Gleason score 2–4 adenocarcinoma of the prostate on needle biopsy: a diagnosis that should not be made. *Am J Surg Pathol* 2000; **24**: 477–8

Correspondence: Hiroji Uemura, Department of Urology, Yokohama City University Graduate School of Medicine, 3–9 Fukuura, Kanazawa-ku, Yokohama 236-0004, Japan.
e-mail: hu0428@med.yokohama-cu.ac.jp

Abbreviations: **ISUP**, International Society of Urologic Pathology; **RP**, radical prostatectomy; **(C)(I)GS**, (conventional) (ISUP) Gleason score; **NB**, needle biopsy; **BRFS**, biochemical recurrence-free survival.

aPKC / promotes growth of prostate cancer cells in an autocrine manner through transcriptional activation of interleukin-6

Hitoshi Ishiguro[a,b], Kazunori Akimoto[c], Yoji Nagashima[d,e], Yasuyuki Kojima[f], Takeshi Sasaki[g], Yukari Ishiguro-Imagawa[h], Noboru Nakaigawa[a], Shigeo Ohno[c,e], Yoshinobu Kubota[a,e], and Hiroji Uemura[a,1]

Departments of [a]Urology, [c]Molecular Biology, [d]Molecular Pathology, [f]Gastroenterological Surgery, and [h]Biology and Function in the Head and Neck, Yokohama City University Graduate School of Medicine, 3-9, Fukuura, Kanazawa-ku, Yokohama, Kanagawa 236-0004, Japan; [g]Division of Pathology, Yokohama City University Medical Center, 4-57, Urafune-cho, Minami-ku Yokohama, Kanagawa 232-0024, Japan; [b]Photocatalyst Group, Kanagawa Academy of Science and Technology. 3-2-1, Sakado, Takatsu-ku, Kawasaki, Kanagawa 213-0012, Japan; and [e]Advanced Medical Research Center, Yokohama City University, Yokohama, Kanagawa 236-0004, Japan

Communicated by Tadamitsu Kishimoto, Osaka University, Osaka, Japan, June 25, 2009 (received for review April 8, 2009)

Understanding the mechanism by which hormone refractory prostate cancer (HRPC) develops remains a major issue. Alterations in HRPC include androgen receptor (AR) changes. In addition, the AR is activated by cytokines such as interleukin-6 (IL-6). Atypical protein kinase C (aPKC /) has been implicated in the progression of several cancers. Herein, we provide evidence that aPKC / expression correlates with prostate cancer recurrence. Experiments in vitro and in vivo revealed aPKC / to be involved in prostate cancer cell growth through secretion of IL-6. Further, aPKC / activates transcription of the IL-6 gene through NF B and AP-1. We conclude that aPKC / promotes the growth of hormone independent prostate cancer cells by stimulating IL-6 production in an autocrine manner. Our findings not only explain the link between aPKC / and IL-6, implicated in the progression a variety of cancers, but also establish a molecular change involved in the development of HRPC. Further, aPKC / expression might be a biomarker for prostate cancer progression.

IL-6 PSA recurrence

Despite earlier detection and recent advances in surgery and radiation, prostate cancer is the second leading cause of cancer deaths in men in western countries (1). Hormone therapy in the form of medical or surgical castration remains the mainstay of systemic prostate cancer treatment. However, despite initial favorable responses to hormone therapy, hormone refractory tumors develop for which there is as yet no effective treatment (2). The androgen receptor (AR) and its signaling remain intact, as demonstrated by the expression of prostate specific antigen (PSA), in androgen-independent cancer cells. Alterations in these cells include AR amplification, AR point mutations, and changes in the expressions of AR co-regulatory proteins (3). In addition, AR can be activated in a ligand-independent fashion by compounds including growth factors and cytokines, such as interleukin-6 (IL-6) (4–6). Understanding the mechanism of androgen-independent prostate cancer development is essential not only for diagnosis but also more effective therapy.

Atypical protein kinase C (aPKC / and aPKC) is a protein kinase C isozyme distinct from other classes of this enzyme, structurally and functionally (7, 8). It plays multifunctional roles in cellular maintenance and growth of epithelial cells, for example, signal transduction and cell polarity (9–15). Studies on lung, ovary, colon, and breast cancers have demonstrated a relationship between aPKC / expression and cancer progression and suggest that aPKC / expression might predict poor survival (16–22). There are several reports showing enhanced aPKC expression in human prostate cancer tissues, but the relationship between aPKC / and prostate cancer progression remains unclear (23, 24). Furthermore, the mechanism by which aPKC promotes the progression of a variety of cancers remains uncertain. Then, we focus on aPKC / expression and its roles in prostate cancer.

IL-6, a cytokine involved in immune and hematopoietic activities, has been implicated in the progression of a variety of human cancers (25). In prostate cancer, IL-6 has been suggested to play a role in cancer progression, especially that of hormone refractory cancer (26–30). Serum IL-6 is elevated in patients with prostate cancer (28). The IL-6 receptor is expressed in prostate cancer cell lines and IL-6 is secreted only by androgen independent prostate cancer cell lines (27, 29, 30). Although these observations suggest the importance of IL-6 in prostate cancer progression, the mechanism by which IL-6 expression is regulated in prostate cancer cells is not fully understood.

Herein, we investigated aPKC / expression in 29 clinical prostate cancer tissue specimens and found a correlation between aPKC / expression and PSA failure, a clinical hallmark of recurrence. Experiments, both in vitro and in vivo, on androgen-independent cancer cells, employing siRNA-mediated depletion of aPKC / , revealed this isozyme to be involved in the proliferation of prostate cancer cells. The in vitro experiments further showed aPKC / involvement in the secretion of IL-6 into the culture medium, suggesting cancer cell growth to occur via an autocrine mechanism. This finding demonstrates the link between aPKC / and IL-6, both of which have been implicated in cancer progression. We also demonstrated that aPKC / is involved in transcription of the IL-6 gene promoter through activation of NF B and AP-1, both of which have been implicated in transcription of the IL-6 gene in prostate cancer cells. We conclude that aPKC / promotes prostate cancer cell growth in an autocrine manner via stimulation of IL-6 production and secretion.

Results

Correlation Between aPKC / Expression and PSA Failure, a Clinical Marker of Prostate Cancer Recurrence. To clarify the relationship between aPKC / expression and prostate cancer, we first evaluated aPKC / expression at the mRNA levels in 29 specimens of human prostate cancer tissues. Clinicopathological features are listed at Table S1. Real-time quantitative PCR (qPCR) analyses revealed that aPKC / mRNA was more highly expressed in cancer tissue samples than in paired normal controls

Author contributions: H.I., K.A., Y.N., and Y. Kubota designed research; H.I., K.A., Y.N., Y. Kojima, T.S., Y.I.-I., and N.N. performed research; H.I., K.A., Y.N., S.O., Y. Kubota, and H.U. analyzed data; and H.I., K.A., Y.N., S.O., Y. Kubota, and H.U. wrote the paper.

The authors declare no conflict of interest.

[1]To whom correspondence should be addressed: E-mail: hu0428@med.yokohama-cu.ac.jp.

This article contains supporting information online at www.pnas.org/cgi/content/full/0907044106/DCSupplemental.

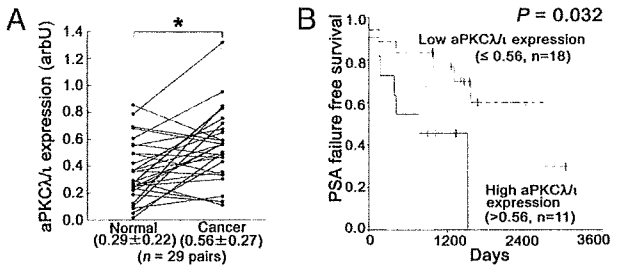

Fig. 1. Relationships between aPKC / expression in prostate cancer tissues. (*A*) aPKC / expression was compared between paired prostate cancer and normal (BPH) prostate tissues obtained from same patients (n 29 pairs). *, P 0.001 by paired t test. arbU: arbitrary units. Values indicate medians SD. (*B*) Kaplan-Meier and log rank analysis of aPKC / and PSA failure time. aPKC / expressions in prostate cancer tissues (n 29) were divided into two groups according to the median value (High: n 11, 0.56 and Low: n 18, 0.56), and analyzed (P 0.032 by log rank test).

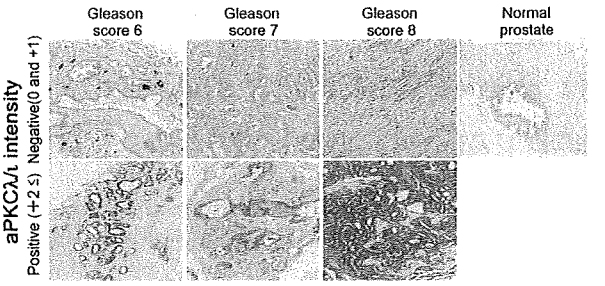

Fig. 2. Representative examples of immunohistochemistry of aPKC / expression. Expression intensities of aPKC / were divided in two groups (positive; 2 and negative; 0 and 1). Gleason scores are indicated in the figures and aPKC / expression in normal prostate tissue is also shown in the figure.

from same patients (Fig. 1*A*, P 0.001). There were no associations between aPKC / mRNA expression and certain clinical features (Fig. S1). On the other hand, when the samples were divided into two groups by setting a cut-off at the median aPKC / value (high: 0.56, n 11 and low: 0.56, n 18), we recognized a statistically significant correlation between aPKC / mRNA expression and PSA failure (Fig. 1*B*, P 0.032). There was no correlation between other clinical features and PSA failure (Fig. S2). Serum PSA was measured every 2–3 months after radical prostatectomy. PSA failure was defined as a continuous elevation with a PSA level greater than 0.2 ng/mL. PSA failure has been suggested to be associated with cancer specific death (31). Thus, aPKC may be a prognostic biomarker for prostate cancer. In univariate and multivariate analyses, only aPKC / mRNA expression showed statistical significance (Table 1, P 0.039 in univariate and P 0.033 in multivariate analysis). Subsequent immunohistochemical analysis of aPKC / in 43 prostate specimens (cancer tissues; n 40, and normal tissues; n 3) confirmed aPKC / expression at the protein level in normal and tumor tissues, with a variety of intensities (Fig. 2 and Table S2). Immunohistochemical analysis also revealed enhanced staining of aPKC / to be localized to the cytoplasm in epithelial cells of the prostate, but not in stromal cells, suggesting the importance of the specific expression of aPKC / protein in epithelial cells of the prostate.

Suppression of aPKC / Expression Reduces Prostate Cancer Cell Growth In Vitro and In Vivo. The correlation of aPKC / expression in prostate cancer tissue samples with PSA failure prompted us to clarify the role of aPKC / in prostate cancer cell lines. Western blot clearly showed aPKC / expression to be higher in prostate cancer cell lines, LNCaP, PC-3 and DU145 cells, than in normal prostate cells, PrEC, as expected (Fig. 3*A*). To evaluate the role of aPKC / in cell growth, we introduced siRNA for aPKC / into the DU145, an androgen-independent cell line, and established a mixture of cell lines expressing siRNA for aPKC / (DU-P), as well as vector control (DU-C) cells. As shown in Fig. 3*B*, we confirmed the reduced expression of aPKC / in the pooled transfectant (DU-P), as compared to control cells (DU-C). We found that DU-P cells grew more slowly than control cells (Fig. 3*C*, P 0.05 at days 3 and 4, and P 0.01 at days 5 and 6). We next transplanted the cell lines into nude mice and monitored the tumor volume in vivo. As shown in Fig. 3*D*, the xenografts of aPKC / -depleted DU-P cells showed slower growth than those of control DU-C cells (P 0.04 at 5 weeks, P 0.012 at 6 weeks). The suppression of aPKC / expression in xenografts was confirmed by RT-PCR analysis (Fig. 3*E*, P 0.001). Thus, the suppression of aPKC / expression leads to the inhibition of prostate cancer growth in vitro and in vivo, clearly indicating a positive role of aPKC / in the growth of prostate cancer cells.

aPKC / Mediates the Growth of Prostate Cancer Cells in an Autocrine Manner Through IL-6 Secretion. To explore the mechanism involved in aPKC / -dependent growth of prostate cancer cells, we

Table 1. Relative hazard of recurrence free survival in univariate and multivariate analysis

		Univariate			Multivariate		
		HR	95% CI	P	HR	95% CI	P
aPKC / expression	0.56 (n 18)						
	0.56 (n 11)	3.914	1.071–14.305	0.039	6.768	1.161–39.443	0.033
Stage	pT2 (n 16)						
	pT3 (n 13)	2.866	0.747–10.992	0.125	3.928	0.781–19.748	0.097
Histology	Well (n 5)						
	Moderately (n 13)	1.129	0.218–5.848	0.885	1.12	0.173–7.275	0.905
	poorly (n 11)	0.892	0.161–4.932	0.895	0.887	0.081–9.669	0.922
Gleason score	6 (n 11)						
	7 (n 10)	1.087	0.291–4.060	0.901	1.562	0.275–8.876	0.615
	8 and 9 (n 8)	0.842	0.184–3.866	0.825	4.346	0.346–54.581	0.255
Age	68 (n 16)						
	68 (n 13)	1.362	0.393–4.718	0.626	1.946	0.488–7.761	0.346
PSA	10 (n 15)						
	10 (n 14)	1.168	0.375–3.639	0.789	0.931	0.233–3.721	0.920

CI, confidence interval; HR, hazard ratio.

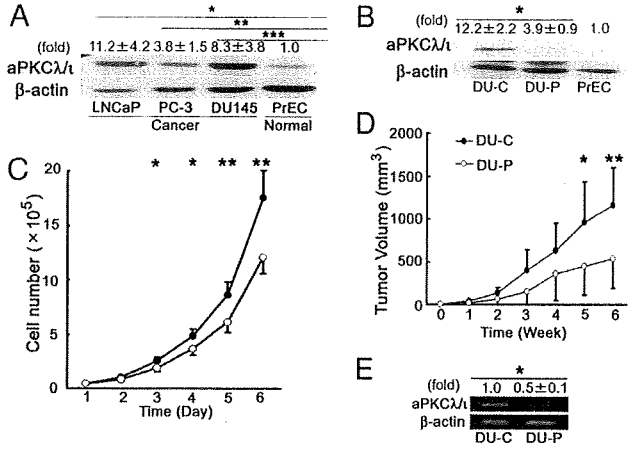

Fig. 3. aPKC / expression in prostate cancer cell lines and growth inhibition of aPKC / siRNA transfected DU145 cells in vitro and in vivo. (*A*) aPKC / expression in prostate cell lines was analyzed by Western blot. -actin was used as an internal control. Values indicate means SD at least three independent experiments (set as 1.0 in PrEC). *, *P* 0.017, **, *P* 0.032 and ***, *P* 0.031 by unpaired *t* test. (*B*) DU145 cells transfected with siRNA for aPKC / expression vector (DU-P cells) and empty vector (DU-C cells) were confirmed by Western blot. -actin was used as an internal control. Values indicate means SD from at least three independent experiments (set as 1.0 in PrEC). *, *P* 0.004 by unpaired *t* test. (*C*) The inhibition of cell growth of siRNA transfected cells in vitro. DU-C (filled circles) and DU-P (open circles) cells were seeded onto 12-well plates at 4 10^4 cells and counted until day 6 (*n* 4 in each group). Points and bars indicate means SD from at least three independent experiments. *, *P* 0.05 **, *P* 0.01 by unpaired *t* test. (*D*) The inhibition of cell growth of siRNA transfected cells in vivo. DU-C (filled circles) and DU-P (open circles) cells were implanted s.c. into the right and left flanks of male nude mice (*n* 7 in each group) and tumor growth was calculated at 6 weeks (The day of injection was taken as week 0). Points and bars indicate means SD. *, *P* 0.04; **, *P* 0.012 by unpaired *t* test. (*E*) aPKC / mRNA expression extracted from xenografts. Total RNA was extracted from the same tumor specimens and aPKC / mRNA expression was examined. Values indicate means SD from at least three independent experiments (set as 1.0 in DU-C derived tumors) *, *P* 0.001 by unpaired *t* test.

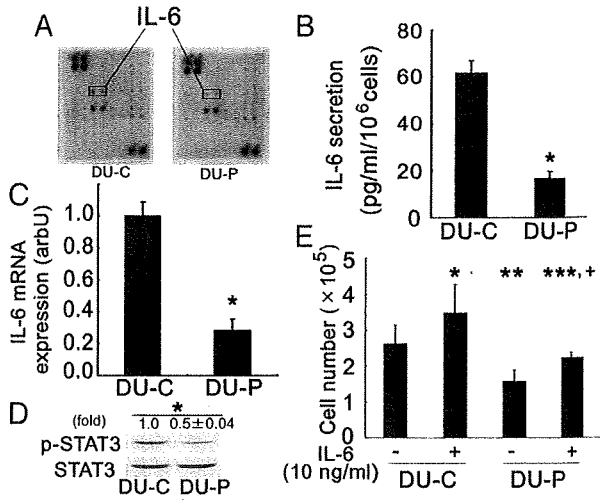

Fig. 4. IL-6 expression was suppressed in siRNA transfected prostate cancer cells. (*A*) Conditioned media from DU-C and DU-P cells were analyzed using a membrane array. Arrows show IL-6 spots. Since this representative data are screening test only, it is performed once. This data had confirmed using ELISA and qPCR. (*B*) Expressions of IL-6 protein in DU-C and DU-P cells were confirmed using ELISA. Conditioned media from DU-C and DU-P (*n* 2 in each group) were analyzed using an IL-6 ELISA kit from R&D Systems. Bars represent means SD from at least three independent experiments. *, *P* 0.002 by unpaired *t* test. (*C*) Expressions of IL-6 mRNA in DU-C and DU-P cells. IL-6 mRNA expression was investigated by qPCR (*n* 3 in each group). Bars represent means SD from at least three independent experiments. *, *P* 0.001 by unpaired *t* test. arbU: arbitrary units. (*D*) STAT3 phosphorylations in DU-C and DU-P cells were analyzed by Western blot. After phospho-STAT3 protein had been detected, membranes were re-probed for STAT-3, and then used as controls. Values indicate means SD at least three independent experiments (set as 1.0 in DU-C). *, *P* 0.002 by unpaired *t* test. (*E*) Recombinant IL-6 stimulated growth of DU-C and DU-P cells. DU-C and DU-P cells were stimulated with IL-6 (10 ng/ml). At day 3 after stimulation, cells were treated with trypsin and counted (*n* 4 in each group). Bars represent means SD from at least three independent experiments. *, *P* 0.001, **, *P* 0.001 and ***, *P* 0.393 (vs. DU-C without IL-6 stimulation) , *P* 0.016 (vs. DU-P without IL-6 stimulation) by ANOVA followed by Bonferroni test.

focused on cytokines which have been implicated in the growth of a variety of cancer cells. Comparison of the conditioned medium between DU-C and DU-P cell lines by cytokine membrane array revealed IL-6 to be a candidate cytokine, that is, that its regulation might be under the control of aPKC / (Fig. 4*A*). The ELISA results confirmed that IL-6 is secreted into conditioned medium of control DU-C cells and decreased in aPKC / -depleted DU-P cells (Fig. 4*B*, *P* 0.002). Similarly, qPCR revealed IL-6 mRNA expression to also be suppressed in aPKC-depleted DU-P cells (Fig. 4*C*, *P* 0.001). These results show that aPKC / regulates IL-6 secretion in prostate cancer cells.

IL-6 is the cytokine reportedly expressed in androgen-independent prostate cancer cell lines including parental DU145 (26, 30). We next examined the effect of aPKC / depletion on phosphorylation of STAT3, one of the downstream mediators of the possible IL-6 involvement in prostate cancer cells (25, 29, 32, 33). As shown in Fig. 4*D*, STAT3 phosphorylation was down-regulated in DU-P cells as compared to DU-C cells, indicating that IL-6 signaling is altered in aPKC / -depleted cells. Given that aPKC / depletion results in the decreased production of IL-6, these results raise another question as to whether aPKC / depletion also affects IL-6 signaling, versus only IL-6 production. To clarify this issue, we next evaluated the response of cells to ectopic IL-6. When both cell types were treated with recombinant IL-6 (10 ng/ml) for 3 days, IL-6 increased cell growth, as we expected (Fig. 4*E*, *P* 0.001 and *P* 0.016). Moreover, DU-P cells treated with IL-6 showed growth similar to that of DU-C cells not treated with IL-6 (Fig. 4*E*, *P* 0.393). Thus, aPKC / depletion does not affect the growth response of cells to IL-6. Taking these observations together, we conclude that secretion of IL-6 enhanced by aPKC / expression plays a role in promoting growth of the prostate cancer cell line DU145. Our results suggest that this growth promotion is mediated in an autocrine manner.

aPKC / Mediates IL-6 Gene Transcription Through NF B and AP-1 in Prostate Cancer Cells. To analyze the mechanism by which aPKC / enhances IL-6 secretion, we next examined the effect of aPKC / on transcription of the IL-6 gene by luciferase reporter assay and EMSA. The luciferase reporter gene, pGL4-IL6p, contains a 1.2-kb 5 -flanking region of genomic DNA isolated from DU145 cells. This region contains the regulatory sequences recognized by AP-1, NF B, MRE and other factors (30). As shown in Fig. 5*A*, overexpression of aPKC / in DU145 cells enhanced activation of the IL-6 promoter (Fig. 5*A*, *P* 0.016). On the other hand, depletion of aPKC / (DU-P cells) resulted in decreased reporter gene expression (Fig. 5*B*, *P* 0.001). These results strongly support the notion that aPKC / is involved in transcription of the IL-6 gene. Transcription of this gene is regulated by two major transcription factors, AP-1 and NF B, in prostate cancer cells (30). To examine the involvement of these transcription factors in aPKC / -mediated IL-6 gene

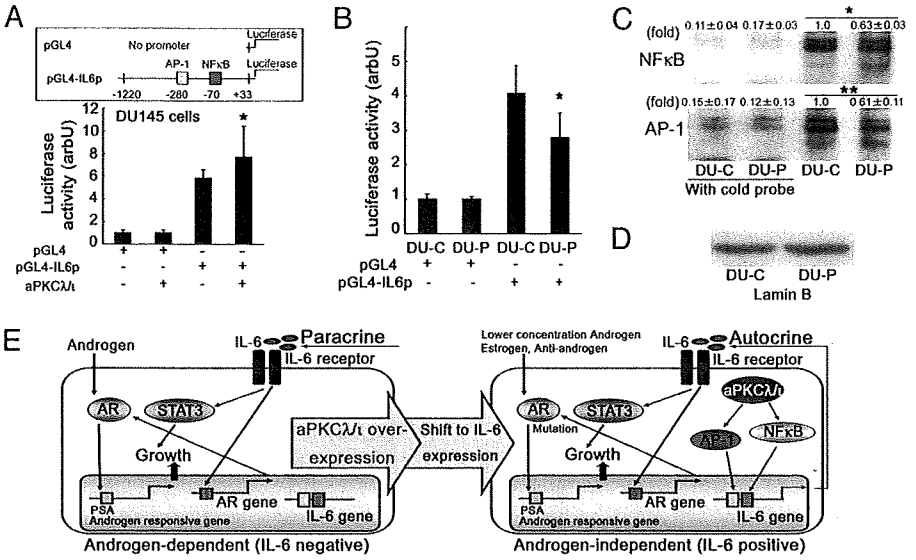

Fig. 5. Involvement of aPKC / in activation of the IL-6 gene promoter and its transcription factors, NF B and AP-1. (*A*) IL-6 promoter activation was induced by wild type aPKC / in DU145 cells. DU145 cells were transfected with pGL4, pGL4-IL6p, empty vector and wild type aPKC / . After a 48 h incubation, luciferase activity was analyzed in a luminometer (*n* 4 in each group). Each control was given a value of 1.0 and each bar indicates the means SD of at least three independent experiments. *, *P* 0.016 (vs. pGL4-IL6p without wild-type aPKC / expression vector) by ANOVA following Bonferroni test. (*B*) IL-6 promoter activation was reduced in DU-P cells. DU-C and DU-P cells were transfected with pGL4 and pGL4-IL6p. After a 12-h incubation, luciferase activity was analyzed in a luminometer (*n* 4 in each group). Each control was given a value of 1.0 and each bar indicates the means SD of at least three independent experiments. *, *P* 0.001 (vs. DU-C with pGL4-IL6p transfection) by ANOVA following Bonferroni test. (*C*) DNA binding properties of NF B and AP-1 were examined by EMSA. Each nuclear extract was reacted with ^{32}P-labeled specific probes. To confirm specific binding of nuclear extracts and probes, reactions were also carried out using a cold probe. Values indicate means SD at least three independent experiments (set as 1.0 in DU-C). *, *P* 0.001 and **, *P* 0.026 by ANOVA following Bonferroni test. (*D*) Nuclear extracts for EMSA were confirmed by lamin B immunoblot. (*E*) Autocrine mechanism of prostate cancer cell growth involving aPKC / and IL-6. Overexpression of aPKC / in prostate cancer cells leads to up-regulation of IL-6 transcription through NF B and AP-1 activation. Secreted IL-6 stimulates cell growth through STAT3 activation in an autocrine manner.

transcription, we used EMSA. The results showed both NF B and AP-1 to be reduced upon aPKC / depletion (Fig. 5 *C* and *D*, *P* 0.001 and *P* 0.026). These results support the notion that both AP-1 and NF B are involved in aPKC / -mediated transcriptional activation of the IL-6 gene.

Discussion

aPKC / overexpression has been implicated in the progression and invasiveness of several tumor types including non-small cell lung cancer, ovarian cancer, breast cancer and glioma (16–22, 34, 35). Gene amplification of aPKC / is also observed in some cases (16, 18). In this study, we obtained evidence supporting a statistically significant correlation between aPKC / overexpression and a clinical marker of prostate cancer recurrence, PSA failure. A very recent study demonstrated aPKC / expression is required for cell survival (36). Thus, the aPKC / expression level and its activity might be prognostic factors for PSA failure.

IL-6, as noted above, has been implicated in the progression of a variety of tumors including prostate cancer (25–27, 29). Its overexpression has been detected in tissues (37, 38) and serum (28) from cancer patients. Preoperative plasma IL-6 level is related to PSA failure after radical prostatectomy (39). In vivo study indicates an important role of IL-6 in prostate cancer cells. Inhibition of IL-6 by anti-IL-6 antibody decreases the growth of PC-3 cells, which is one of an androgen-independent prostate cancer cells, in vivo (40). Therefore, IL-6 may play a role in androgen-independent growth of prostate cancer. Our findings on the molecular link between aPKC / and IL-6 raise an intriguing question as to the correlation between aPKC / expression and IL-6 expression in prostate cancer patients. We evaluated our tissue samples for IL-6 expression by qPCR. However, there was no statistically significant correlation between aPKC / expression and IL-6 expression (Fig. S3). One explanation is that the examined tissues contained not only cancer cells but also stromal cells. In support of this possibility, most prostate cancer tissues that express high levels of aPKC / protein (30/43, 70%) show a specific overexpression in epithelial cells but not in the surrounding stromal cells. However, IL-6 is reportedly expressed not only in prostate cancer epithelial cells, but also in stromal cells (37, 38). Thus, the use of laser capture microdissection (LCM) might be required to clarify this point. Unfortunately, we did not have sufficient sample quantities for LCM. We are currently conducting more extensive clinical studies aimed at clarifying the correlation between aPKC / expression and IL-6 expression.

Experiments using the prostate cancer cell line DU145 revealed that aPKC / is involved in prostate cancer growth both in vivo and in vitro. Furthermore, depletion of aPKC / in DU145 cells suppressed NF B and AP-1 activities, transcription and secretion of IL-6, as well as suppressing cell growth, but not IL-6 signaling. We conclude that enhanced aPKC / expression in prostate cancer cells results in overproduction and secretion of a prostate growth factor, IL-6, at the transcriptional level. This forms an autocrine loop contributing to the growth of prostate cancer (Fig. 5*E*). The aPKC-dependent expression of IL-6 mRNA is also observed for another androgen-independent prostate cell line, PC-3, suggesting the generality of this regulation (Fig. S4). The specific overexpression of aPKC / in epithelial cells but not in stromal cells of the prostate further supports such an autocrine mechanism. It is known that most of androgen-independent prostate cancer tissues overexpress or/ and express mutated AR that is still activated by lower concentration androgen, estrogen and anti-androgen drug (3). Taken together, the pathway might cooperate with the deregulated AR

system to regulate proliferation of hormone-independent prostate cancer cells (Fig. 5*E*).

The following reports strongly support our conclusion. Combined constitutive activation of NF B and AP-1 has been reported to mediate deregulated expression of IL-6 in DU145 cells (30). Ectopic expression of IL-6 in IL-6-negative LNCaP prostate cancer cells results in stimulation of the STAT3 signaling pathway as well as cell growth (29). However, the mechanism by which IL-6 expression is deregulated is not yet fully understood. As for aPKC / , several studies have shown that aPKC / activates NF B and AP-1 (9, 10, 13–15, 41–44). Furthermore, aPKC activates NF B in prostate cells (45). aPKC deregulates the growth of mouse prostate cancer cells (46). While the mechanism by which aPKC affects the growth of cancer cells remains obscure, the involvement of Rho B suppression in aPKC-dependent invasive properties in glioblastoma (35) and that of activation of the Rac1/Erk pathway in aPKC-dependent growth and tumorigenicity have been reported (17, 22). Our present results may explain the link between aPKC / and IL-6, two molecules implicated in the progression of a variety of malignancies, and establish a molecular mechanism underlying prostate cancer development and/or progression, thereby providing insights into the prognosis and treatment of prostate cancer.

How aPKC / expression was regulated in prostate cancer cells? Amplification of aPKC / gene is reported in lung and ovarian cancer (16, 18, 19) and amplification of chromosome 3q including aPKC / gene in prostate cancer cell lines (47). Another possibility is that aPKC / expression is up-regulated through the transcriptional activation of aPKC / promoter during hormone refractory process. Gustafson et al. reported aPKC / promoter analysis using luciferase (48). They show Bcr-Abl regulates aPKC / expression through the MEK-dependent activation of an Elk1 element within aPKC / promoter in leukemia cell line. We are ongoing the investigation of the mechanism of aPKC / overexpression involving in hormone refractory process. Further, other molecules expression, such as PAR-4, might be affected the alteration of aPKC / activity during hormone refractory process (49).

One of the most important clinical aspects of prostate cancer is dramatically decreased androgen-dependent cell growth, a typical indicator of prostate cancer progression. Possible mechanisms include androgen receptor overexpression and other mutations that result in hypersensitivity to androgens and/or other growth factors (3–6). IL-6 is overexpressed in hormone refractory prostate cancer patients and is one of the factors implicated in this process (26–28, 37). Importantly, IL-6 can stimulate androgen receptor activation independently of androgens with the induction of androgen receptor expression (4, 5). A recent study on LNCaP cells, which are sensitive to androgens and do not usually express IL-6, suggested IL-6 to be involved in the progression of prostate cancer cells from androgen dependence to androgen independence (50). It has been reported androgen-dependent prostate cancer cells obtained from xenografts treated with the anti-IL-6 antibody retained in androgen-dependence. In contrast, cancer cells obtained from xenografts untreated with the anti-IL-6 antibody are converted to androgen-independence in vitro and in vivo experiments, which means that IL-6 contributes to the development of androgen independence in prostate cancer (51). Taking these observations and our results together, we speculate that the molecular link between aPKC / and IL-6 revealed in the present study supports the notion that aPKC / is involved in this transition from androgen dependent to androgen independent growth of prostate cancer. As for the relationship between androgens and aPKC, there is an interesting report suggesting that aPKC , another aPKC isotype, is involved in the growth of androgen dependent LNCaP cells (52). In LNCaP cells, androgen stimulates aPKC through an unknown mechanism, and AILNCaP, a LNCaP subline established after androgen depletion, showed constitutive activation of aPKC . Another study on a breast cancer cell line, MCF7, showed the involvement of aPKC in estradiol-dependent cell growth (53). These reports further suggest a close relationship between aPKC and hormone-dependent cell growth. Our present findings provide additional evidence clarifying this point and are anticipated to facilitate understanding the progression of hormone-related malignancies including prostate cancer. Furthermore, aPKC / expression might be a biomarker for prostate cancer progression.

Materials and Methods

Cell Lines, Patients, and Tissues Sample. LNCaP, PC-3, and DU145 cells were obtained from the American Type Culture Collection. PrEC cells were obtained from Clonetics. All cell lines were maintained with suitable medium (F-12 supplemented with 10% FCS (FCS) for LNCaP and PC-3, MEM supplemented with 10% FCS for DU145, PrEGM for PrEC) under 5% CO_2.

Paired human untreated primary prostate cancer tissues and normal (or benign prostatic hypertrophy (BPH)) (*n* 29) tissues from same patients were obtained during radical prostatectomy at Yokohama City University Hospital and its affiliates. The sampling and usage of all prostate tissues in this study were approved by the ethical committee of Yokohama City University Graduate School of Medicine and performed only after obtaining informed consent from each patient. For details, see *SI Text* and Table S1.

Reagents. Human recombinant IL-6 was purchased from R&D Systems. G418 was purchased from Invitrogen Corp. Anti-aPKC antibody was purchased from BD Biosciences. Anti-lamin-B antibody (c-19) was purchased from Santa Cruz Biotechnology Inc. Anti-actin antibody (AC-15) was purchased from Sigma-Aldrich. Anti-phospho-STAT3 and anti-STAT3 (#9131 and #9132, respectively) antibodies were purchased from Cell Signaling Technology Inc. Anti-rabbit and anti-mouse horseradish peroxidase conjugates were purchased from GE Healthcare U.K. Ltd.

Generation of Stable Transfectant-Induced siRNA for aPKC / . To investigate the role of aPKC / in prostate cancer, we generated aPKC / knock-down cells using siRNA for aPKC / . The pEB6-Super vector (54) encoding the shRNA sequence for aPKC / RNAi with the target sequence 5 -CAA GTG TTC TGA AGA GTT T-3 (DU-P cells) or empty vector (DU-C cells) was transfected into DU145 cells using Nucleofactor electroporation methods (Amaxa AG). Then, transfected cells were selected by G418 (800 g/mL) over a 3-week period. After the specific down-regulation of aPKC / had been confirmed by Western blot, the cells were used for further experiments.

RNA Extraction and Real-Time Quantitative PCR (qPCR). Total RNA from cell lines, prostate tissues and xenografts were extracted using ISOGEN (Nippon-Gene) according to the manufacturer's instructions. After cDNA had been synthesized with random hexomers and MMLV (Moloney Murine Leukemia Virus), qPCR was performed with an iCycler and SYBR Green Supermix (Bio-Rad). For details, see *SI Text*.

Immunohistochemistry. Immunohistochemistry was performed for aPKC / protein expression according to the previous report (20). For details, see *SI Text*.

Cell Growth Analysis. DU-C or DU-P cells (4 10^4) were incubated in 12-well plates (day 0). Incubated cells were harvested with trypsin and counted till 6 days (from day 1 to day 6) using a hematocytometer (Beckman Coulter, Inc.). For the IL-6 stimulation experiment, 4 10^4 DU-C or DU-P cells were seeded onto 12-well plates and incubated for 24 h. The medium was then changed to phenol red-free RPMI1640 with 0.1% BSA (BSA), IL-6 (10 ng/mL) was added and incubation was continued for another 3 days. Then, cells were harvested with trypsin and counted.

In Vivo Tumor Growth. 5 10^6 cells (DU-C and DU-P cells) were injected into the flank regions of athymic nude mice (4–6 weeks old, *n* 7). Tumors were measured weekly with a caliper (for comparison with the week 0 value). The tumor volume was calculated using the formula: tumor volume (mm^3) 0.5 length (width)^2. After 6 weeks, tumors were isolated and aPKC / expression was confirmed by RT-PCR.

Cytokine Membrane Array. Cytokines in the conditioned medium were detected using Human Cytokine Array III (Ray Biotech) according to the manufacturer's instructions. For details, see *SI Text*.

ELISA (ELISA) for IL-6 Secretion. IL-6 secretion in the collected medium was measured using a human IL-6 ELISA kit according to the manufacturer's instructions (R&D Systems). For details, see *SI Text*.

Western Blot. Cell lysates were prepared and subjected to Western blot. For details, see *SI Text*.

Luciferase Assay. Approximately 1.2 kb of the IL-6 5 -flanking region was generated using PCR from genomic DNA extracted from DU145 cells, and cloned into the pGL4.0 [*luc2*] vector (pGL4-IL6p) (Promega). Wild type aPKC / was obtained as described in previous reports (9, 10). phRL-SV40 was used as the internal control for the luciferase assay (Promega). After cells transfected each plasmid vector were incubated and lysed, luciferase activity was measured using the dual-luciferase reporter assay system (Promega) and a luminometer, TD-20/20 (Turner Design). For details, see *SI Text*.

Electrophoretic Mobility Shift Assay (EMSA). Nuclear proteins of DU-C or DU-P were extracted using NE-PER (Pierce Biotechnology Inc.) and subjected to EMSA using gel shift assay systems (Promega). For details, see *SI Text*.

Statistical Analysis. All statistical analyses were performed using SPSS for windows (SPSS Inc.). For details, see *SI Text*.

ACKNOWLEDGMENTS. We thank R. Shimizu, Y. Nakamura, T. Yamaki, Y. Imano, T. Taniguchi, H. Soeda, C. Kondo, and A. Ishiyama for technical and secretarial assistance. This work was supported by Grants-in-Aid for Scientific Research from the Ministry of Education, Culture, Science, and Technology; a COE Research Grant from the Japan Society for the Promotion of Science; and a Grant for Strategic Research Promotion from Yokohama City University.

1. Jemal A, et al. (2007) Cancer statistics, 2007. *CA Cancer J Clin* 57:43–66.
2. Calabrò F, Sternberg CN (2007) Current indications for chemotherapy in prostate cancer patients. *Eur Urol* 51:17–26.
3. Taplin ME, Balk SP (2004) Androgen receptor: A key molecule in the progression of prostate cancer to hormone independence. *J Cell Biochem* 91:483–490.
4. Culig Z, Bartsch G, Hobisch A (2002) Interleukin-6 regulates androgen receptor activity and prostate cancer cell growth. *Mol Cell Endocrinol* 197:231–238.
5. Lin DL, Whitney MC, Yao Z, Keller ET (2001) Interleukin-6 induces androgen responsiveness in prostate cancer cells through up-regulation of androgen receptor expression. *Clin* Cancer Res 7:1773–1781.
6. Zhu ML, Kyprianou N (2008) Androgen receptor and growth factor signaling cross-talk in prostate cancer cells. *Endocr Relat Cancer* 15:841–849.
7. Akimoto K, et al. (1994) A new member of the third class in the protein kinase C family, PKC lambda, expressed dominantly in an undifferentiated mouse embryonal carcinoma cell line and also in many tissues and cells. *J Biol Chem* 269:12677–12683.
8. Nishizuka Y (1995) Protein kinase C and lipid signaling for sustained cellular responses. *FASEB J* 9:484–496.
9. Akimoto K, et al. (1996) EGF or PDGF receptors activate atypical PKC through phosphatidylinositol 3-kinase. *EMBO J* 15:788–798.
10. Akimoto K, et al. (1998) Atypical protein kinase C binds and regulates p70 S6 kinase. *Biochem J* 335:417–424.
11. Suzuki A, Akimoto K, Ohno S (2003) Protein kinase C / (PKC /): aPKC isotype essential for the development of multicellular organism. *J Biochem* 133:9–16.
12. Ohno S (2001) Intercellular junctions and cellular polarity: The PAR-aPKC complex, a conserved core cassette playing fundamental roles in cell polarity. *Curr Opin Cell Biol* 13:641–648.
13. Diaz-Meco MT, et al. (1993) A dominant negative protein kinase C zeta subspecies blocks NF-kappa B activation. *Mol Cell Biol* 13:4770–4775.
14. Moscat J, Diaz-Meco MT, Albert A, Campuzano S (2006) Cell signaling and function organized by PB1 domain interactions. *Mol Cell* 23:631–640.
15. Sanz L, Sanchez P, Lallena MJ, Diaz-Meco MT, Moscat J (1999) The interaction of p62 with RIP links the atypical PKCs to NF B activation. *EMBO J* 18:3044–3053.
16. Regala RP, et al. (2005) Atypical protein kinase C is an oncogene in human non-small cell lung cancer. *Cancer Res* 65:8905–8911.
17. Regala RP, et al. (2005) Atypical protein kinase C plays a critical role in human lung cancer cell growth and tumorigenicity. *J Biol Chem* 280:31109–31115.
18. Eder AM, et al. (2005) Atypical PKC iota contributes to poor prognosis through loss of apical-basal polarity and cyclin E overexpression in ovarian cancer. *Proc Natl Acad Sci USA* 102:12519–12524.
19. Zhang L, et al. (2006) Integrative genomic analysis of protein kinase C (PKC) family identifies PKCiota as a biomarker and potential oncogene in ovarian carcinoma. *Cancer Res* 66:4627–4635.
20. Kojima Y, et al. (2008) The overexpression and altered localization of the atypical Protein kinase C lambda/iota in breast cancer correlates with the pathological type of these tumors. *Human Pathol* 39:824–831.
21. Li Q, et al. (2008) Correlation of aPKC-iota and E-cadherin expression with invasion and prognosis of cholangiocarcinoma. *Hepatobiliary Pancreat Dis Int* 7:70–75.
22. Murray NR, et al. (2004) Protein kinase C is required for Ras transformation and colon carcinogenesis in vivo. *J cell Biol* 164:797–802.
23. Cornford P, et al. (1999) Protein kinase C isoenzyme patterns characteristically modulated in early prostate cancer. *Am J Pathol* 154:137–144.
24. Koren R, et al. (2004) Expression of protein kinase C isoenzymes in benign hyperplasia and carcinoma of prostate. *Oncol Rep* 11:321–326.
25. Hong DS, Angelo LS, Kurzrock R (2007) Interleukin-6 and its receptor in cancer: implications for translational therapeutics. *Cancer* 110:1911–1928.
26. Okamoto M, Lee C, Oyasu R (1997) Interleukin-6 as a paracrine and autocrine growth factor in human prostatic carcinoma cells in vitro. *Cancer Res* 57:141–146.
27. Corcoran NM, Costello AJ (2003) Interleukin-6: Minor player or starring role in the development of hormone-refractory prostate cancer ? *BJU Int* 91:545–553.
28. Nakashima J, et al. (2000) Serum interleukin 6 as a prognostic factor in patients with prostate cancer. *Clin* Cancer Res 6:2702–2706.
29. Lou W, Ni Z, Dyer K, Tweardy DJ, Gao AC (2000) Interleukin-6 induces prostate cancer cell growth accompanied by activation of stat3 signaling pathway. *Prostate* 42:239–242.
30. Zerbini LF, Wang Y, Cho JY, Libermann TA (2003) Constitutive activation of nuclear factor B p50/p65 and Fra-1 and JunD is essential for deregulated interleukin 6 expression in prostate cancer. *Cancer Res* 63:2206–2215.
31. Freedland SJ, et al. (2005) Risk of prostate cancer-specific mortality following biochemical recurrence after radical prostatectomy. *JAMA* 294:433–439.
32. Heinrich PC, et al. (2003) Principles of interleukin (IL)-6-type cytokine signaling and its regulation. *Biochem J* 374:1–20.
33. Tam L, et al. (2007) Expression levels of the JAK/STAT pathway in the transition from hormone-sensitive to hormone-refractory prostate cancer. *Br J Cancer* 97:378–383.
34. Patel R, et al. (2008) Involvement of PKC-iota in glioma proliferation. *Cell Prolif* 41:122–135.
35. Baldwin RM, Parolin DA, Lorimer IA (2008) Regulation of glioblastoma cell invasion by PKC iota and RhoB. *Oncogene* 27:3587–3595.
36. Win HY, Acevedo-Duncan M (2009) Role of protein kinase C-iota in transformed non-malignant RWPE-1 cells and androgen-independent prostate carcinoma DU-145 cells. *Cell Prolif* 42:182–194.
37. Hobisch A, et al. (2000) Immunohistochemical localization of interleukin-6 and its receptor in benign, premalignant and malignant prostate tissue. *J Pathol* 191:239–244.
38. Royuela M, et al. (2004) Immunohistochemical analysis of the IL-6 family of cytokines and their receptors in benign, hyperplasic, and malignant human prostate. *J Pathol* 202:41–49.
39. Shariat SF, et al. (2001) Plasma levels of interleukin-6 and its soluble receptor are associated with prostate cancer progression and metastasis. *Urology* 58:1008–1015.
40. Smith PC, Keller ET (2001) Anti-interleukin-6 monoclonal antibody induces regression of human prostate cancer xenografts in nude mice. *Prostate* 48:47–53.
41. Huang C, et al. (2001) Inhibition of atypical PKC blocks ultraviolet-induced AP-1 activation by specifically inhibiting ERKs activation. *Mol Carcinog* 27:65–75.
42. Lu Y, Jamieson L, Brasier AR, Fields AP (2001) NF-kappaB/RelA transactivation is required for atypical protein kinase C iota-mediated cell survival. *Oncogene* 20:4777–4792.
43. Bonizzi G, Piette J, Schoonbroodt S, Merville MP, Bours V (1999) Role of the protein kinase C / isoform in nuclear factor- B activation by interleukin-1 or tumor necrosis ' factor-≤ cell type specificities. *Biochem Pharmacol* 57:713–720.
44. Lallena MJ, Diaz-Meco MT, Bren G, Payá CV, Moscat J (1999) Activation of I B kinase by protein kinase C isoforms. *Mol Cell Biol* 19:2180–2188.
45. Win HY, Acevedo-Duncan M (2008) Atypical protein kinase C phosphorylates IKK≤ in transformed non-malignant prostate cell survival. *Cancer Lett* 270:302–311.
46. Ghosh PM, Bedolla R, Mikhailova M, Kreisberg JI (2002) RhoA-dependent murine prostate cancer cell proliferation and apoptosis: Role of protein kinase Czeta. *Cancer Res* 62:2630–2636.
47. Nupponen NN, Hyytinen ER, Kallioniemi AH, Visakorpi T (1998) Genetic alterations in prostate cancer cell lines detected by comparative genomic hybridization. *Cancer Genet Cytogenet* 101:53–57.
48. Gustafson WC, et al. (2004) Bcr-Abl regulates protein kinase C (PKC) transcription via an Elk1 site in the PKC promoter. *J Biol Chem* 279:9400–9408.
49. Gurumurthy S, Rangnekar VM (2004) Par-4 inducible apoptosis in prostate cancer. *J Cell Biol* 91:504–512.
50. Lee SO, Chun JY, Nadiminty N, Lou W, Gao AC (2007) Interleukin-6 undergoes transition from growth inhibitor associated with neuroendocrine differentiation to stimulator accompanied by androgen receptor activation during LNCaP prostate cancer cell progression. *Prostate* 67:764–773.
51. Wallner L, et al. (2006) Inhibition of interleukin-6 with CNTO328, an anti-inteleukin-6 monoclonal antibody, inhibits conversion of androgen-dependent prostate cancer to an androgen-independent phonotype in orchiectomized mice. *Cancer Res* 66:3087–3095.
52. Inoue T, et al. (2006) Requirement of androgen-dependent activation of protein kinase C for androgen-dependent cell proliferation in LNCaP cells and its roles in transition to androgen-independent cells. *Mol Endocrinol* 20:3053–3069.
53. Castoria G, et al. (2004) Role of atypical protein kinase C in estradiol-triggered G1/S progression of MCF-7 cells. *Mol Cell Biol* 24:7643–7653.
54. Suzuki A, et al. (2004) aPKC acts upstream of PAR-1b in both the establishment and maintenance of mammalian epithelial polarity. *Curr Biol* 14:1425–1435.

Avid F-18 FDG Uptake in Prostatic Sarcoma

Ryogo Minamimoto, MD, PhD, Ukihide Tateishi, MD, PhD,* Hiroji Uemira, MD, PhD,† Shoji Yamanaka, MD, PhD,‡ Yoshinobu Kubota, MD, PhD,† and Tomio Inoue, MD**

Abstract: We report the F-18 FDG PET appearance of an adult prostatic sarcoma. A 76-year-old man with a history of prostate cancer treated by hormone therapy, a lobulated heterogeneous mass in the prostate gland was found on a follow-up pelvic computed tomography. Although the prostate-specific antigen level was within the normal range, transperineal core needle biopsy was performed because recurrent prostatic carcinoma was suspected. The tumor was pathologically diagnosed as a prostatic sarcoma with no evidence of existing prostatic carcinoma. F-18 FDG-PET revealed avid-FDG uptake (maximum SUV of 7.1) and no evidence of distant metastasis.

Key Words: prostatic sarcoma, [F-18]fluorodeoxyglucose, positron emission tomography

(*Clin Nucl Med* 2009;34: 388–389)

Received for publication December 25, 2008; accepted February 8, 2009.

From the Departments of *Radiology, and †Urology, Graduate School of Medicine, Yokohama City University, Yokohama, Japan; and ‡Division of Anatomic and Surgical Pathology, Hospital of Yokohama City University, Yokohama City University School of Medicine, Yokohama, Japan.

Reprints: Ryogo Minamimoto, MD, PhD, Department of Radiology, Yokohama City University, Graduate School of Medicine, 3-9 Fukuura, Kanazawa-ku, Yokohama-shi, Kanagawa-ken, Japan 236-0004. E-mail: ryogom@yokohama-cu.ac.jp.

ISSN: 0363-9762/09/3406-0388

REFERENCES

1. D'Amico AV, Chen MH, Cox MC, et al. Prostate-specific antigen response duration and risk of death for patients with hormone-refractory metastatic prostate cancer. *Urology*. 2005;66:571–576.
2. Schröder FH, van der Cruijsen-Koeter I, de Koning HJ, et al. Prostate cancer detection at low prostate specific antigen. *J Urol*. 2000;163:806–812.
3. Young MD, Dahm P, Robertson CN. Prostatic sarcoma with rapid tumor progression after nerve sparing radical cystoprostatectomy. *J Urol*. 2001;166: 994.
4. Schwarzbach MH, Dimitrakopoulou-Strauss A, Willeke F, et al. Clinical value of [18-F] fluorodeoxyglucose positron emission tomography imaging in soft tissue sarcomas. *Ann Surg*. 2000;231:380–386.
5. Umesaki N, Tanaka T, Miyama M, et al. Positron emission tomography with (18)F-fluorodeoxyglucose of uterine sarcoma: a comparison with magnetic resonance imaging and power Doppler imaging. *Gynecol Oncol*. 2001;80: 372–377.
6. Sung J, Espiritu JI, Segall GM, et al. Fluorodeoxyglucose positron emission tomography studies in the diagnosis and staging of clinically advanced prostate cancer. *BJU Int*. 2003;92:24–27.
7. Hricak H, Choyke PL, Eberhardt SC, et al. Imaging prostate cancer: a multidisciplinary perspective. *Radiology*. 2007;243:28–53.
8. Kao PF, Chou YH, Lai CW. Diffuse FDG uptake in acute prostatitis. *Clin Nucl Med*. 2008;33:308–310.
9. Ho L, Quan V, Henderson R, et al. High-grade urothelial carcinoma of the prostate on FDG PET-CT. *Clin Nucl Med*. 2007;32:746–747.
10. Sexton WJ, Lance RE, Reyes AO, et al. Adult prostate sarcoma: the M. D. Anderson Cancer Center Experience. *J Urol*. 2001;166:521–525.

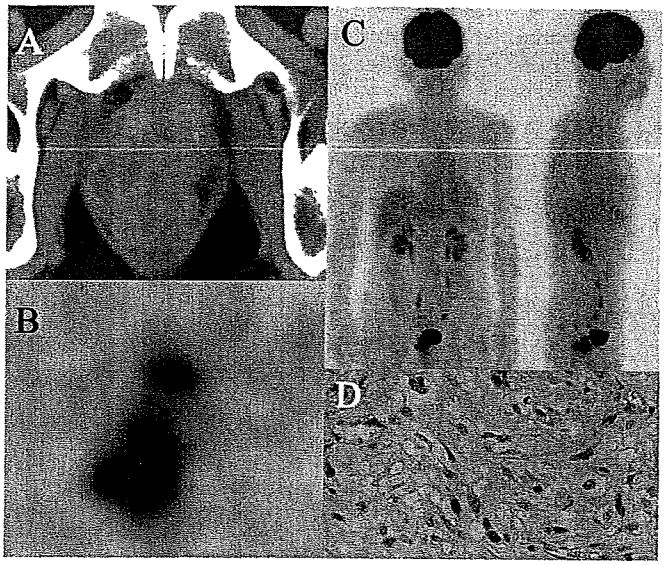

FIGURE 1. A 76-year-old man with a history of prostate cancer found to have a lobulated heterogeneous mass in the prostate gland on a follow-up pelvic computed tomography (CT). In this case, the primary prostate cancer had been treated with hormone therapy alone. Although the prostate-specific antigen (PSA) level, a marker of prostate cancer recurrence, was "undetectable" (0.3 ng/mL), the possibility of prostate cancer relapse could not be ruled out because recurrent prostate cancer has been observed in patients with low PSA levels.[1,2] The tumor was pathologically diagnosed as a prostatic sarcoma. Following this, F-18 fluorodeoxyglucose (FDG) positron emission tomography (PET) scan was performed for survey. **A,** The computed tomography scan showed a lobulated heterogeneous mass arising from the prostate gland. **B,** The transverse view of an F-18 FDG-PET scan at 60 minutes after FDG injection revealed avid-FDG uptake (maximum SUV of 7.1) corresponding to this mass. **C,** A whole body F-18 FDG-PET scan showed high FDG uptake in the prostate grand and no evidence of distant metastasis. **D,** A pathologic specimen of the prostate tumor, obtained by transperineal core needle biopsy and stained with hematoxylin and eosin, is shown. The pathologic image demonstrated overgrowth of spindle-shaped cells with hyperchromatic nuclei and frequent atypical mitosis surrounded by myxoid stroma. The tumor was immunoreactive for vimentin, P53, and ki-67, and negative for PSA. The tumor was pathologically diagnosed as a prostatic sarcoma with no evidence of existing prostatic carcinoma.

Prostatic sarcoma is extremely rare, representing only 0.1% of all prostatic neoplasms.[3] In this case, the prostatic sarcoma showed avid-FDG uptake; this has also been reported in sarcomas arising in other parts of the human body.[4,5] On the other hand, it has been reported that F-18 FDG-PET has limited value in the evaluation of prostate cancer.[6,7]

A sarcoma should be considered in the differential diagnosis, along with prostatitis and urothelial carcinoma, in cases with avid-FDG uptake on an F-18 FDG PET scan of the prostate gland.[8,9] Moreover, an F-18 FDG PET scan can be advantageous in cases of prostatic sarcoma for identifying distant metastasis, which commonly occurs and is associated with reduced survival.[10] As this case had no evidence of metastasis, intensity-modulated radiation therapy was selected for treatment.

Int. J. Radiation Oncology Biol. Phys., Vol. 69, No. 1, pp. 194–203, 2007

0360-3016/07/$–see front matter

ELSEVIER

doi:10.1016/j.ijrobp.2007.05.026

BIOLOGY CONTRIBUTION

HIGH RELATIVE BIOLOGIC EFFECTIVENESS OF CARBON ION RADIATION ON INDUCTION OF RAT MAMMARY CARCINOMA AND ITS LACK OF H-*RAS* AND *TP53* MUTATIONS

TATSUHIKO IMAOKA, PH.D.,* MAYUMI NISHIMURA,* SHIZUKO KAKINUMA, PH.D.,* YUKIKO HATANO,* YASUSHI OHMACHI, D.V.M., PH.D.,* SHINJI YOSHINAGA, PH.D.,† AKIHIRO KAWANO, D.V.M.,‡‖ AKIHIKO MAEKAWA, M.D., PH.D.,‖ AND YOSHIYA SHIMADA, PH.D.*

*Experimental Radiobiology for Children's Health Research Group, Chiba, Japan; †Regulatory Sciences Research Group, and ‡Department of Technical Support and Development, National Institute of Radiological Sciences, Chiba, Japan; and ‖Chemical Management Center, National Institute of Technology and Evaluation, Tokyo, Japan

Purpose: The high relative biologic effectiveness (RBE) of high-linear energy transfer (LET) heavy-ion radiation has enabled powerful radiotherapy. The potential risk of later onset of secondary cancers, however, has not been adequately studied. We undertook the present study to clarify the RBE of therapeutic carbon ion radiation and molecular changes that occur in the rat mammary cancer model.

Methods and Materials: We observed 7–8-week-old rats (ACI, F344, Wistar, and Sprague-Dawley) until 1 year of age after irradiation (0.05–2 Gy) with either 290 MeV/u carbon ions with a spread out Bragg peak (LET 40–90 keV/μm) generated from the Heavy-Ion Medical Accelerator in Chiba or ^{137}Cs γ-rays.

Results: Carbon ions significantly induced mammary carcinomas in Sprague-Dawley rats but less so in other strains. The dose–effect relationship for carcinoma incidence in the Sprague-Dawley rats was concave downward, providing an RBE of 2 at a typical therapeutic dose per fraction. In contrast, ~10 should be considered for radiation protection at low doses. Immunohistochemically, 14 of 18 carcinomas were positive for estrogen receptor α. All carcinomas examined were free of common H-*ras* and *Tp53* mutations. Importantly, lung metastasis (7%) was characteristic of carbon ion–irradiated rats.

Conclusions: We found clear genetic variability in the susceptibility to carbon ion–induced mammary carcinomas. The high RBE for carbon ion radiation further supports the importance of precise dose localization in radiotherapy. Common point mutations in H-*ras* and *Tp53* were not involved in carbon ion induction of rat mammary carcinomas. © **2007 Elsevier Inc.**

Heavy-ion radiotherapy, High linear energy transfer radiation, Rat mammary carcinogenesis, Relative biologic effectiveness, *Tp53* and H-*ras* mutations.

INTRODUCTION

Heavy-ion radiotherapy is expected to improve cancer treatment results by achieving accurate dose localization and a high relative biologic effectiveness (RBE) because of the sharp Bragg peak and high linear energy transfer (LET) of the radiation. The Lawrence Berkeley National Laboratory in the United States, the Gesellschaft für Schwerionenforschung in Germany, and the National Institute of Radiological Sciences (NIRS) in Japan have performed clinical trials for heavy-ion cancer therapy. Since 1994, clinical studies at NIRS have been conducted using carbon ion radiation from

Reprint requests to: Tatsuhiko Imaoka, Ph.D., Experimental Radiobiology for Children's Health Research Group, National Institute of Radiological Sciences, 4-9-1 Anagawa, Inage-ku, Chiba 263-8555, Japan. Tel: (+81) 43-206-3221; Fax: (+81) 43-206-4138; E-mail: t_imaoka@nirs.go.jp

Supported in part by a Grant-In-Aid for Cancer Research (Grant 16S-1) and a Grant for Anticancer Project (Grant 19141201) from the Ministry of Health, Labor and Welfare of Japan; a Grant-In-Aid for Scientific Research from the Japan Society for Promotion of Science (Grant 13470263); an LRI grant from Japan Chemical Industry Association (Grant 2006CC03-01); a grant from Ground-Based Research Announcement for Space Utilization Research from Japan Space Forum (Grant 17-031-18); and a Grant for Basic Science Research Projects from the Sumitomo Foundation (Grant 060611).

A. Kawano is presently at Yamaguchi Prefectural Headquarter, National Federation of Agricultural Co-operative Associations.

Conflict of interest: none.

Acknowledgments—The authors thank J. Nagai, M. Ootawara, H. Osada, H. Moritake, S. Sasaki, Y. Amasaki, M. Okabe, U. Enzaka, T. Honda, and R. Sakamoto for technical assistance; the Laboratory Animal Sciences Section, National Institute of Radiological Sciences, for animal management; and E. Obara, Y. Sugawara, F. Mizumoto, and H. Saito for secretarial help. This study is a part of the Research Project with Heavy Ions at National Institute of Radiological Sciences-heavy-ion medical accelerator in Chiba (No. 14B239).

Received Aug 18, 2006, and in revised form May 15, 2007. Accepted for publication May 15, 2007.

the Heavy-Ion Medical Accelerator in Chiba (HIMAC) (1). Because of the primarily narrow Bragg peak, spread out Bragg peaks (SOBPs) have been devised to obtain broad and uniform dose distributions (2). The carbon ion radiation of 290 MeV/u with 6-cm SOBPs has been successfully used to treat several cancer types (3). Using this particular treatment lends itself to more accurate control of cancer and longer patient survival compared with conventional radiotherapy regimens. As a result, however, the potential risk of developing secondary cancers is now becoming a matter of concern, and it is important to determine the RBE value of therapeutic heavy ions for inducing late occurring cancers.

Epidemiologic studies of atomic bomb survivors and irradiated patients have suggested that the mammary glands are among the most susceptible organs to radiation-induced cancers (4–6). Substantial amounts of experimental animal data, especially with rat models, also complement these epidemiologic studies. Previous animal studies have shown that mammary tissues have extremely high RBE values for carcinogenesis, ranging from 10 to >100, when using high-LET neutrons (7–9). Thus, it is predicted that therapeutic carbon ions could also have a high RBE because of the high LET, although little evidence exists for potential carcinogenicity of heavy ions on this particular type of cancer (10, 11).

It is well established that the genetic makeup influences cancer susceptibility. Genetic factors play an important role in determining the susceptibility to rat mammary tumor formation, whether by radiation or chemical carcinogens (9, 12–15). These data suggest that exposure to carbon ions is an important risk factor for breast cancer, the susceptibility to which largely depends on the genetic background of the exposed subject. To date, however, no study has examined the importance of genetic background on heavy-ion–induced mammary carcinogenesis.

In the present study, we aimed at providing two RBE values, one for risk estimation of therapies and the other for consideration in radiation protection. We first used four rat strains to investigate the effect on mammary carcinogenicity of carbon ions of 290 MeV/u with 6-cm SOBPs from the HIMAC. On identification of the Sprague-Dawley rat as susceptible, we then studied the dose–effect relationship and calculated the RBE. The carcinomas were then further analyzed for their molecular features such as estrogen receptor (ER)α status and mutations in the genes H-*ras* and *Tp53*. We found that carbon ions induced rat mammary carcinomas in a strain-dependent manner. An RBE value of 2 was appropriate for risk estimation of therapeutic doses, and a value of $\sim$10 should be considered in protection against low doses. We also found that most carcinomas were positive for ERα and that all tumors examined lacked H-*ras* and *Tp53* mutations.

METHODS AND MATERIALS

Heavy-ion and γ-ray irradiation

The carbon ion irradiation experiments were conducted at the HIMAC in NIRS, using a 290-MeV/u carbon ion beam with 6-cm SOBPs (1). Each rat was placed in a 5-cm-wide polymethylmethacrylate chamber such that the center of the chamber was positioned in the middle of the SOBP (LET, 40–90 keV/μm) (2). The duration of irradiation ranged from 1 to 2 min, resulting in an average dose rate of 0.1–1.0 Gy/min. γ-Irradiation was performed as described previously using a ^{137}Cs γ-irradiator at a dose rate of 0.6 Gy/min (16).

Animal experiments

All animals were treated in accordance with the Safety and Health Regulations for Handling Experimental Animals compiled by the Safety and Ethical Handling Regulations Committee for Laboratory Animal Experiments, NIRS. For the strain-dependent experiments, 5-week-old female rats of inbred ACI (ACI/N Jcl) and F344 (F344/Jcl) strains and outbred Sprague-Dawley (Jcl:SD) and Wistar (Jcl:Wistar) strains were purchased from Clea Japan (Tokyo, Japan). They were housed in autoclaved cages and maintained in rooms with a controlled temperature (23° $\pm$ 1°C) and humidity (45% $\pm$ 5%) under a regular 12-h light, 12-h dark cycle. They were fed a standard laboratory animal diet (MB-1, Oriental Yeast, Tokyo, Japan) and sterilized water *ad libitum*. At 8 weeks of age, the rats underwent whole-body irradiation with carbon ions of 0, 0.5, 1, and 2 Gy. The treated rats were observed daily, and periodic palpation was started at 10 weeks after irradiation. The animals that became moribund during the observation period were killed and the mammary tumors were collected from them, as well as from those that had died. After 1 year, the observation period was complete, and the surviving animals were killed using ether anesthesia followed by sample collection for experimentation (16). For the dose–effect experiments, 5-week-old Sprague-Dawley rats were purchased and housed as described above and fed a standard laboratory animal diet (CE-2, Clea Japan). At 7 weeks of age, they underwent whole-body irradiation with either carbon ions of 0.05, 0.1, 0.2, 0.5, 1, and 2 Gy or ^{137}Cs γ-rays of 0.5, 1, and 2 Gy (n = 20–29), as described above. A control group (n = 45) remained unirradiated. A portion of the results on the control (n = 36) and γ-ray (2 Gy, n = 20) groups has been published previously (16). The treated rats were fed a high corn oil (23.5%) AIN-76A diet (Clea Japan) from 9 weeks of age and palpated weekly. At 1 year of age, the rats with palpable tumors were killed using ether anesthesia. The excised tumors were fixed in 10% neutral-buffered formalin, and 2-μm-thick paraffin-embedded sections were routinely prepared and stained with hematoxylin and eosin for histologic evaluation. Mammary tumors were diagnosed as either adenocarcinomas or benign tumors, including fibroadenomas and adenomas (17). Portions of the mammary tumors were snap frozen in liquid nitrogen and stored at −80°C for genomic DNA analyses.

ERα immunohistochemistry

Immunohistochemistry was performed using an antibody against ERα (MC-20, Santa Cruz Biotechnology, Santa Cruz, CA) as follows. Rehydrated specimens were subjected to antigen retrieval by autoclaving at 120°C for 20 min in 10 mM sodium citrate buffer (pH 6.0). Endogenous peroxidase was quenched in 0.3% hydrogen peroxide/methanol for 15 min. Nonspecific binding was blocked with a mixture of 10% normal goat serum (Cedarlane Laboratories, Ontario, Canada) and 4% skim milk (Block Ace, Dainippon Pharmaceutical, Osaka, Japan). The specimens were incubated at 4°C overnight with anti-ERα (diluted 1:25), washed, and then incubated with a peroxidase-conjugated secondary antibody [Histofine Simple Stain MAX PO(R) kit, Nichirei Biosciences, Tokyo, Japan]. Peroxidase activity was visualized with diaminobenzidine staining (Simple Stain DAB Solution; Nichirei Biosciences). After counterstaining with hematoxylin, the specimens were dehydrated,

mounted, and analyzed. As a negative control, the specimens were also incubated without anti-ERα. The proportion of ERα-positive cells was calculated by dividing the number of stained epithelial cells by the number of total epithelial cells in the same field (~1,600 cells on average). An ERα-positive proportion ≥10% was defined as ERα positive, as has generally been accepted for human and rat mammary cancers (18, 19).

H-ras *mutation analysis by restriction fragment length polymorphism*

Restriction fragment length polymorphism was used to detect H-*ras* mutations in carcinomas, as previously described (20). H-*ras* mutations protect the *MnlI* restriction enzyme site that spans the codon 12/13 junction. In brief, genomic DNA was isolated by phenol-chloroform extraction and purified by ethanol precipitation. A partial sequence of H-*ras* in the purified DNA was amplified by polymerase chain reaction (PCR) and subsequently digested with *MnlI*. The resulting fragments were separated by agarose gel electrophoresis and visualized by ethidium bromide staining.

Tp53 *mutation analysis*

The presence of *Tp53* mutations in carcinomas was determined by PCR, followed by direct sequencing. PCR primers were designed to amplify genomic regions containing exons 5–7. The PCR program consisted of an initial denaturation at 94°C (5 min) followed by 35 cycles of amplification at 94°C (10 s) for denaturation, the annealing temperature as indicated below (30 s), and extension at 72°C (30 s), with a final extension step at 72°C (5 min). The primer sequences and their respective annealing temperatures were as follows: 5′-GTTGGCTTGTCCGCTGACCT-3′ (forward) and 5′-TA AAGAGGGCTGGGCCTGTG-3′ (reverse) at 68°C for a 631-base pair region encompassing exons 5 and 6, and 5′-CTTATCTG TGGCATCTTGGGTTCC-3′ (forward) and 5′-TTGCTGGGGA GAGGAGCTTG-3′ (reverse) at 55°C for a 400-base pair region encompassing exon 7. After agarose gel electrophoresis, amplified fragments were excised, eluted from gels using the Freeze-N-Squeeze Spin Column (Bio-Rad Laboratories, Hercules, CA), and purified by ethanol precipitation. Subsequently, sequencing was performed using the BigDye Terminator Cycle Sequencing FS Ready Reaction kit (Applied Biosystems, Foster City, CA) and analyzed on an ABI 310 Genetic Analyzer (Applied Biosystems).

Statistical analysis

The crude tumor incidence data were analyzed with Fisher's exact probability test. The incidence data were corrected with the Kaplan-Meier method for differences in observation periods resulting from death before 1 year of age. These data were then analyzed with the log–rank test using StatMate III statistics software (Atms, Tokyo, Japan). Tumor multiplicity data, before and after adjustment for the survival period (*i.e.*, division by relative periods under observation), and tumor latency data were analyzed using the Kruskal-Wallis test followed by the Mann-Whitney *U* test. The excess relative risk (ERR) ascribed to irradiation was defined as the corrected tumor incidence in the irradiated group divided by that in the control minus unity. The ERR data were fitted using the maximum likelihood method to a dose-square ($\alpha D^{0.5}$), linear (αD), or linear-quadratic ($\alpha D + \beta D^2$) relationship, where D is the dose in Gray and α and β are constants. The goodness of fit of these data was assessed by the chi-square test. The RBE of carbon ions at a dose D_C was defined as the ratio $D\gamma/D_C$, where γ-rays at the dose $D\gamma$ and carbon ions at the dose D_C gave the same ERR values. The standard errors of the ratio parameters were calculated by the δ method. The measure for statistical significance was $p < 0.05$.

RESULTS

Carbon ions induce rat mammary carcinomas in a strain-dependent manner

To evaluate the effects of heavy-ion therapy on mammary tumor formation, we conducted a carcinogenesis experiment

Table 1. Incidence and multiplicity of mammary carcinomas and benign tumors in ACI, F344, Sprague-Dawley, and Wistar rat strains after exposure to carbon ion radiation

Strain	Dose (Gy)	*n*	Incidence (*n*)		Multiplicity (mean ± SE)	
			Carcinoma	Benign	Carcinoma	Benign
ACI	0	8	1 (13)	0 (0)	0.13 ± 0.13	0
	0.5	8	0 (0)	0 (0)	0	0
	1	8	1 (13)	0 (0)	0.13 ± 0.13	0
	2	8	1 (13)	0 (0)	0.13 ± 0.13	0
F344	0	8	0 (0)	0 (0)	0	0
	0.5	9	0 (0)	0 (0)	0	0
	1	9	0 (0)	0 (0)	0	0
	2	8	0 (0)	1 (13)	0	0.13 ± 0.13
Sprague-Dawley	0	8	0 (0)	1 (13)	0	0.13 ± 0.13
	0.5	9	4 (44)	5 (56)	0.44 ± 0.18*	0.78 ± 0.28*
	1	9	6 (67)†	7 (78)‡	0.89 ± 0.31§	1.11 ± 0.26§
	2	9	4 (44)	6 (67)‡	0.78 ± 0.36*	2.22 ± 0.68§
Wistar	0	8	0 (0)	0 (0)	0	0
	0.5	9	1 (11)	2 (22)	0.11 ± 0.11	0.33 ± 0.24
	1	9	1 (11)	4 (44)	0.11 ± 0.11	0.67 ± 0.29*
	2	9	2 (22)	6 (67)	0.22 ± 0.15	0.89 ± 0.26§

Data in parentheses are percentages.
* $p < 0.05$, Mann-Whitney *U* test.
† $p < 0.01$, Fisher's exact probability test.
‡ $p < 0.05$, Fisher's exact probability test.
§ $p < 0.01$, Mann-Whitney *U* test.

in which four rat strains (Wistar, ACI, F344, and Sprague-Dawley) were irradiated with carbon ions and observed until 1 year of age. The pathologic analysis of the mammary tumors revealed that the treatment induced predominantly malignant papillary and tubular types of adenocarcinomas, in addition to benign fibroadenomas and adenomas (Table 1). More specifically, the Sprague-Dawley rats showed significant development of carcinomas compared with unirradiated rats in a dose-dependent manner at 0.5, 1, and 2 Gy, although induction at 2 Gy was somewhat attenuated. The Wistar and ACI rats sporadically developed mammary carcinomas, and no carcinomas were observed in the F344 rats. Both the Sprague-Dawley and Wistar strains developed benign tumors that were not evident in the ACI or F344 strains. For the Sprague-Dawley rats, the mean duration ± standard deviation between irradiation and palpation of the first carcinomas and benign tumors was 28.7 ± 9.6 and 34.8 ± 5.0 weeks, respectively.

The presence of ERα is usually indicative of tumor hormone dependence (21). Mammary carcinomas (15 from Sprague-Dawley and 3 from Wistar) were analyzed immunohistochemically for ERα expression. Of these 18 tumors, 14 (78%) were positive for ERα (Fig. 1), with the percentage of ERα-immunoreactive cells at 10–36%. Some ERα-immunoreactive cells contacted the basement membrane (Fig. 1A), and others were separated from it by a layer of non–ERα-expressing cells (Fig. 1B), as reported previously for 1-methyl-1-nitrosourea-induced rat mammary carcinoma (18). Four carcinomas showed ERα immunoreactivity in <10% of tumor cells and were hence defined as ERα negative (Fig. 1C). No correlation was found between positive ERα expression and radiation dose.

Dose–effect relationship and RBE of carbon ion–induced mammary carcinogenesis

On identifying the Sprague-Dawley rat as susceptible to carbon ions, we then analyzed the dose–effect relationship in this strain to determine the RBE of carbon ions for mammary cancer induction. We analyzed the incidence and multiplicity of rat mammary carcinomas in response to 0–2 Gy of carbon ions (Table 2 and Fig. 2A,B) and, in addition, the results for benign tumors (Table 3 and Fig. 2C,D). All the data indicated that the dose–effect relationships for both benign and malignant tumors are concave downward for carbon ions, but they are linear for γ-rays. Notably, low doses of carbon ions (0.05 and 0.1 Gy) significantly increased ($p < 0.05$) the carcinoma and benign tumor multiplicities, respectively. Carcinoma multiplicity showed a local peak at 0.05 Gy (Fig. 2B). Kaplan-Meier plots of tumor-free survival for carcinoma (Fig. 3A,B) and benign tumors (Fig. 3C,D) showed that carcinoma development also had a tendency toward earlier onset in the 0.05-Gy group than either the 0- or 0.1-Gy group (Fig. 3A), although the development of benign tumors did not (Fig. 3C). The mean duration between irradiation and first palpation was 23.8 ± 12.0 and 29.2 ± 7.3 weeks for carcinomas (Fig. 3A) and benign tumors (Fig. 3C), respectively.

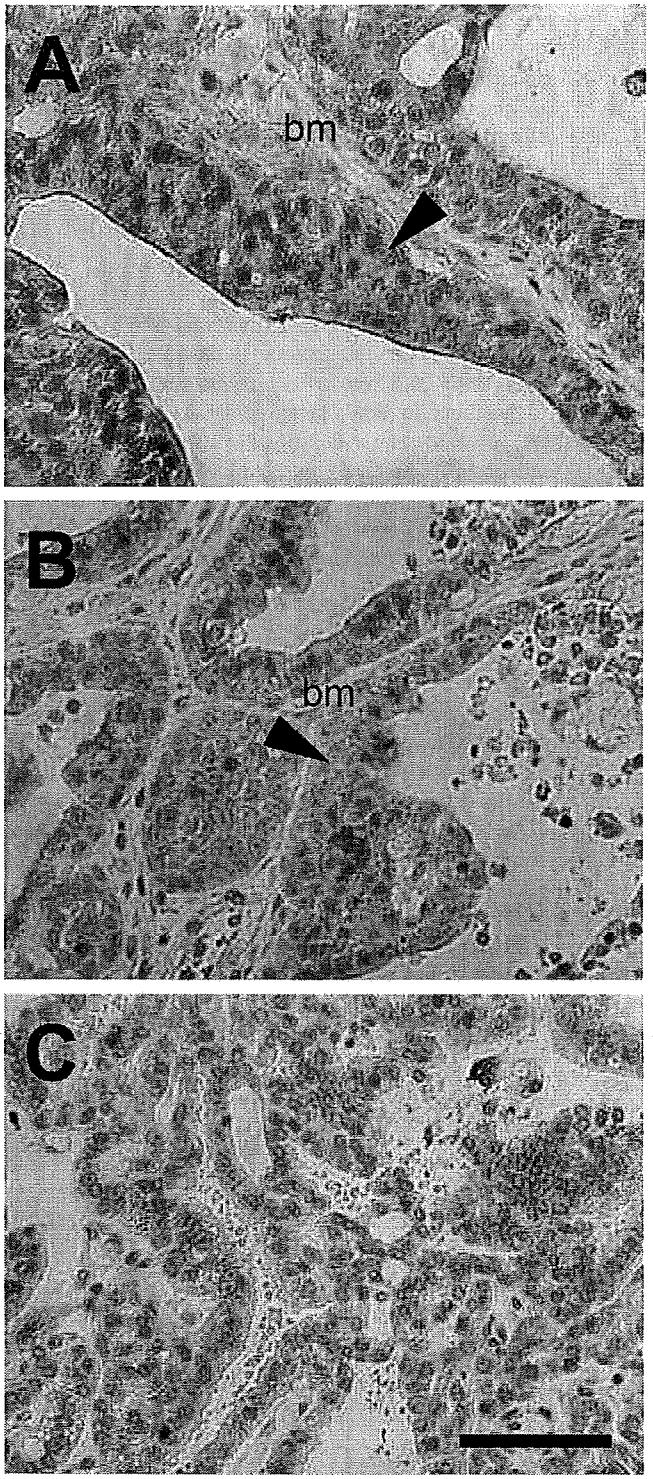

Fig. 1. Immunohistochemistry for estrogen receptor (ER)α in carbon ion–induced rat mammary carcinomas. Tumors were immunostained with anti-ERα (brown staining) and counterstained with hematoxylin. (A,B) Carcinomas with ≥10% of ERα-immunoreactive cells. (A) Some immunoreactive cells (arrowhead) remained in contact with basement membrane (bm), and (B) others were separated from it by layer of nonimmunoreactive cells (arrowhead). (C) Carcinoma with a <10% of ERα-immunoreactive cells. Bar = 25 μm.

We found no significant difference in this duration between the examined dose groups; however, we did observe a significant difference ($p < 0.01$) between malignant and benign

Table 2. Incidence, multiplicity, and period between irradiation and first palpation of mammary adenocarcinoma in Sprague-Dawley rats after exposure to carbon ion radiation and γ-rays

		Incidence			Multiplicity		
Dose (Gy)	*n*	Crude (*n*)	%	Corrected	Crude	Corrected	First palpation (wk)
Control							
0	45	3	7 ± 4	7 ± 4	0.07 ± 0.04	0.07 ± 0.04	32.3 ± 6.8
Carbon ions							
0.05	20	4	20 ± 9	20 ± 9	0.45 ± 0.27*	0.47 ± 0.27*	25.8 ± 12.5
0.1	20	4	20 ± 9	21 ± 9	0.25 ± 0.12	0.25 ± 0.12	36.0 ± 4.2
0.2	20	6	30 ± 10	30 ± 10†	0.35 ± 0.13†	0.40 ± 0.17†	23.5 ± 13.8
0.5	29	12	41 ± 9‡	42 ± 9‡	0.59 ± 0.17‡	0.62 ± 0.17§	22.4 ± 12.6
1	20	12	60 ± 11§	61 ± 11§	1.05 ± 0.23§	1.36 ± 0.35§	18.8 ± 10.4
2	20	13	65 ± 11§	69 ± 11§	1.40 ± 0.39§	1.60 ± 0.43§	20.5 ± 12.5
γ-Rays							
0.5	20	4	20 ± 9	20 ± 9	0.20 ± 0.09	0.21 ± 0.10	26.5 ± 10.1
1	20	6	30 ± 10*	30 ± 10†	0.45 ± 0.17†	0.51 ± 0.19†	24.3 ± 13.7
2	20	11	55 ± 11§	57 ± 12§	0.90 ± 0.24§	1.07 ± 0.30§	26.4 ± 12.5

Data presented as mean ± standard error for incidence and multiplicity and as mean ± standard deviation for first palpation, unless otherwise noted.

* $p < 0.05$.
† $p < 0.01$.
‡ $p < 0.001$.
§ $p < 0.0001$.

tumors. Pathologically, lung metastases were observed in 9 (7%) of 129 rats in the carbon ion groups irrespective of the dose irradiated, but not in any of the 60 rats in γ-ray groups ($p < 0.05$; Table 4).

We adopted the incidence data for calculating RBE because of its consistent increase with dose. Taking into account the microdosimetric feature of high-LET radiation, Kellerer and Rossi (22) made a theoretical explanation for

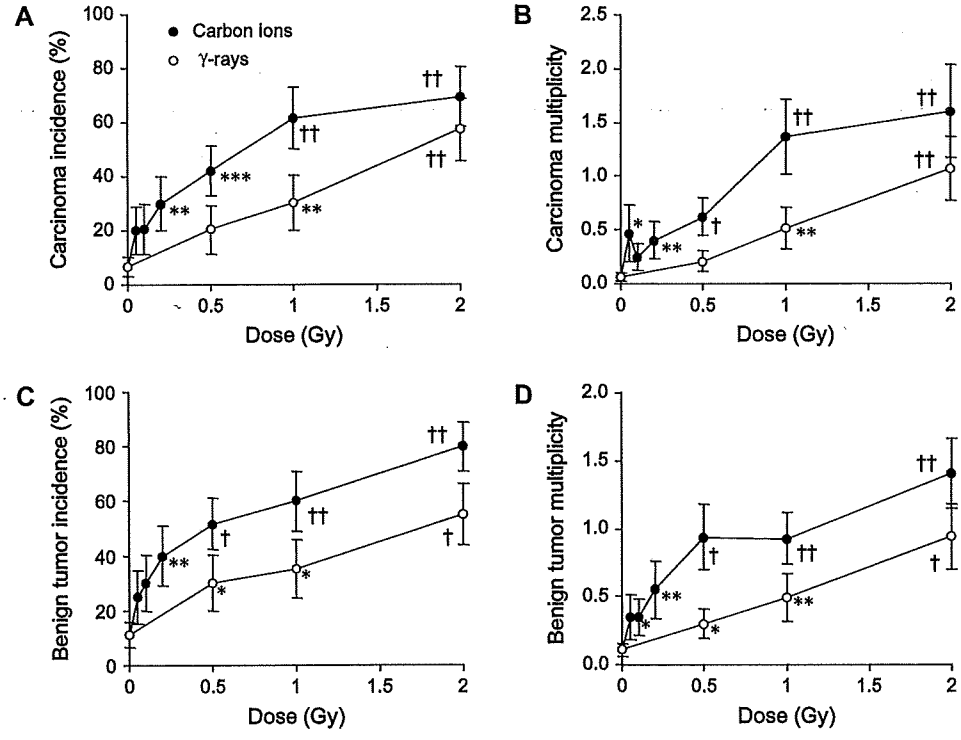

Fig. 2. Dose–effect relationships for rat mammary tumor induction by carbon ions and γ-rays in Sprague-Dawley rats. (A) Incidence of carcinomas adjusted for survival periods with Kaplan-Meier method and comparisons made using the log–rank test. (B) Multiplicity of carcinomas adjusted for survival periods and analyzed with Mann-Whitney *U* test. (C,D) Benign tumor incidence and multiplicity analyzed as Fig. A and B, respectively. *$p < 0.05$, **$p < 0.01$, ***$p < 0.001$, †$p < 10^{-4}$; and ††$p < 10^{-5}$ vs. 0 Gy. Black circles indicate carbon ions and white circles indicate γ-rays. Bars indicate standard error (n = 20–45).

Table 3. Incidence, multiplicity, and period between irradiation and first palpation of mammary fibroadenomas/adenomas in Sprague-Dawley rats after exposure to carbon ion radiation and γ-rays

		Incidence			Multiplicity		
Dose (Gy)	*n*	Crude	%	Corrected	Crude	Corrected	First palpation (wk)
Control							
0	45	5	11 ± 5	11 ± 5	0.11 ± 0.05	0.11 ± 0.05	32.0 ± 5.9
Carbon ions							
0.05	20	5	25 ± 10	26 ± 10	0.35 ± 0.17	0.35 ± 0.17	30.8 ± 6.2
0.1	20	6	30 ± 10	31 ± 11	0.35 ± 0.13*	0.35 ± 0.13*	33.8 ± 6.3
0.2	20	8	40 ± 11†	42 ± 11†	0.55 ± 0.21†	0.55 ± 0.21†	32.1 ± 5.1
0.5	29	15	52 ± 9‡	53 ± 10§	0.93 ± 0.24§	0.94 ± 0.24§	28.5 ± 8.2
1	20	12	60 ± 11	74 ± 12§	0.90 ± 0.19§	0.93 ± 0.19§	26.8 ± 5.4
2	20	16	80 ± 9§	92 ± 8§	1.30 ± 0.23§	1.40 ± 0.26§	26.3 ± 8.4
γ-Rays							
0.5	20	6	30 ± 10	31 ± 11*	0.30 ± 0.11*	0.30 ± 0.11*	28.5 ± 5.9
1	20	7	35 ± 11*	36 ± 11*	0.45 ± 0.15†	0.49 ± 0.17†	29.6 ± 11.2
2	20	11	55 ± 11‡	62 ± 12§	0.90 ± 0.24§	0.94 ± 0.25§	30.3 ± 6.5

Data presented as mean ± standard error for incidence and multiplicity and as mean ± standard deviation for first palpation, unless otherwise noted.

* $p < 0.05$.
† $p < 0.01$.
‡ $p < 0.001$.
§ $p < 0.0001$.

the repeated observation that RBE is inversely proportional to the square root of the dose. Because the dose–effect relationship is linear for mammary cancer induction by low-LET radiation (7, 23, 24), the curve for high-LET radiation can be fitted to a square-root function of dose. This relationship adequately describes the curves of neutron-induced mammary carcinogenesis (7, 8, 23). In the present study, linearity was rejected ($p < 0.001$) for carbon ion–related ERR (ERR_C) of carcinomas and benign tumors within a dose range of 0–2 Gy. Although the linear (0–0.2 Gy, $p = 0.562$) and the

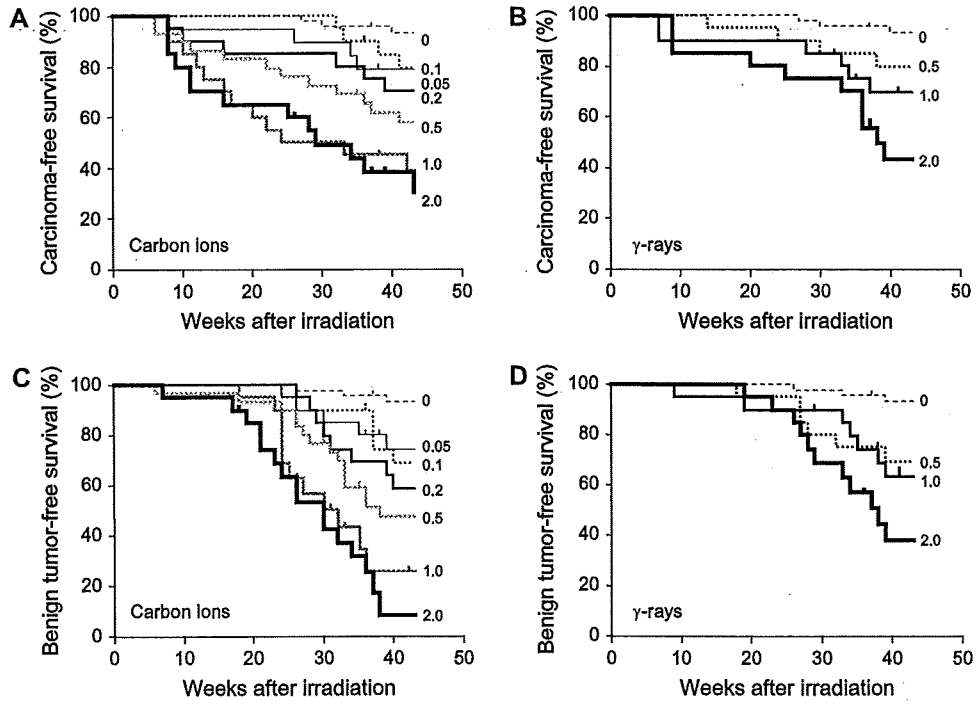

Fig. 3. Time course of rat mammary tumor development after either carbon ion or γ-ray irradiation. Rate of carcinoma-free survival indicated using Kaplan-Meier method for rats irradiated with (A) carbon ions and (B) γ-rays for dose range of 0–2 Gy. Rate of benign tumor-free survival indicated similarly for rats irradiated with (C) carbon ions and (D) γ-rays. Dose in Gray indicated to right of each line.

Table 4. Incidence of lung metastases from mammary carcinoma in Sprague-Dawley rats after exposure to carbon ion radiation and γ-rays

Variable	Dose (Gy)	Incidence	
		Crude	Within carcinoma-bearing rats*
Control	0	0/45 (0)	0/3 (0)
Carbon ions	0.05	1/20 (5)	1/4 (25)
	0.1	0/20 (0)	0/4 (0)
	0.2	1/20 (5)	1/9 (11)
	0.5	3/29 (10)	3/15 (20)
	1	3/20 (15)	3/13 (23)
	2	1/20 (5)	1/16 (6)
Total		9/129† (7)	9/61† (15)
γ-Rays	0.5	0/20 (0)	0/4 (0)
	1	0/20 (0)	0/8 (0)
	2	0/20 (0)	0/12 (0)
Total		0/60 (0)	0/24 (0)

* Included rats with nonpalpable mammary carcinoma; hence, numbers do not necessarily coincide with those in Table 2.
† $p < 0.05$ vs. γ-rays.

linear-quadratic (0–2 Gy, $p = 0.559$) relationships were not rejected, the carcinoma data were best described (0–2 Gy, $p = 0.997$) by a square-root function of

$$ERR_C = \alpha_C D_C^{0.5} \quad (1)$$

where $\alpha_C = 7.193 \pm 0.284$ (mean ± standard error) and D_C is the carbon ion dose in Gray (Fig. 4A). The γ-ray–related ERR (ERR_γ) of carcinomas was adequately described by a linear (0–2 Gy, $p = 0.987$) relationship of

$$ERR_\gamma = \alpha_\gamma D_\gamma \quad (2)$$

where $\alpha_\gamma = 3.726 \pm 0.068$ and D_γ is the γ-ray dose in Gray (Fig. 4A). Using these relationships, the RBE for carbon ion–induced carcinomas was

$$RBE = (\alpha_C/\alpha_\gamma) D_C^{-0.5} \quad (3)$$

where $\alpha_C/\alpha_\gamma = 1.931 \pm 0.084$ (Fig. 4C). This formula gives an RBE value of 1.9 ± 0.1 if $D_C = 1$ and 8.6 ± 0.4 if $D_C = 0.05$.

Similarly, the ERR_C for benign tumors could be fitted to both linear (0–0.2 Gy, $p = 0.784$) and linear-quadratic (0–2 Gy, $p = 0.636$) equations; however, it was best described by the dose–square (0–2 Gy, $p = 1.000$) relationship of Eq. 1, where $\alpha_C = 5.327 \pm 0.123$ (Fig. 4B). The ERR_γ for benign tumors was fitted to the linear (0–2 Gy, $p = 0.859$) relationship of Eq. 2, where $\alpha_\gamma = 2.330 \pm 0.152$ (Fig. 4B). The carbon ion RBE of benign tumor induction was expressed using Eq. 3, where $\alpha_C/\alpha_\gamma = 2.286 \pm 0.159$ (Fig. 4C). This gives an RBE value of 2.3 ± 0.2 for $D_C = 1$ and 10.2 ± 0.7 for $D_C = 0.05$.

*Heavy-ion–induced mammary carcinomas negative for H-*ras *and* Tp53 *mutations*

To date, the molecular characteristics for heavy-ion–induced mammary carcinomas remain to be reported. The

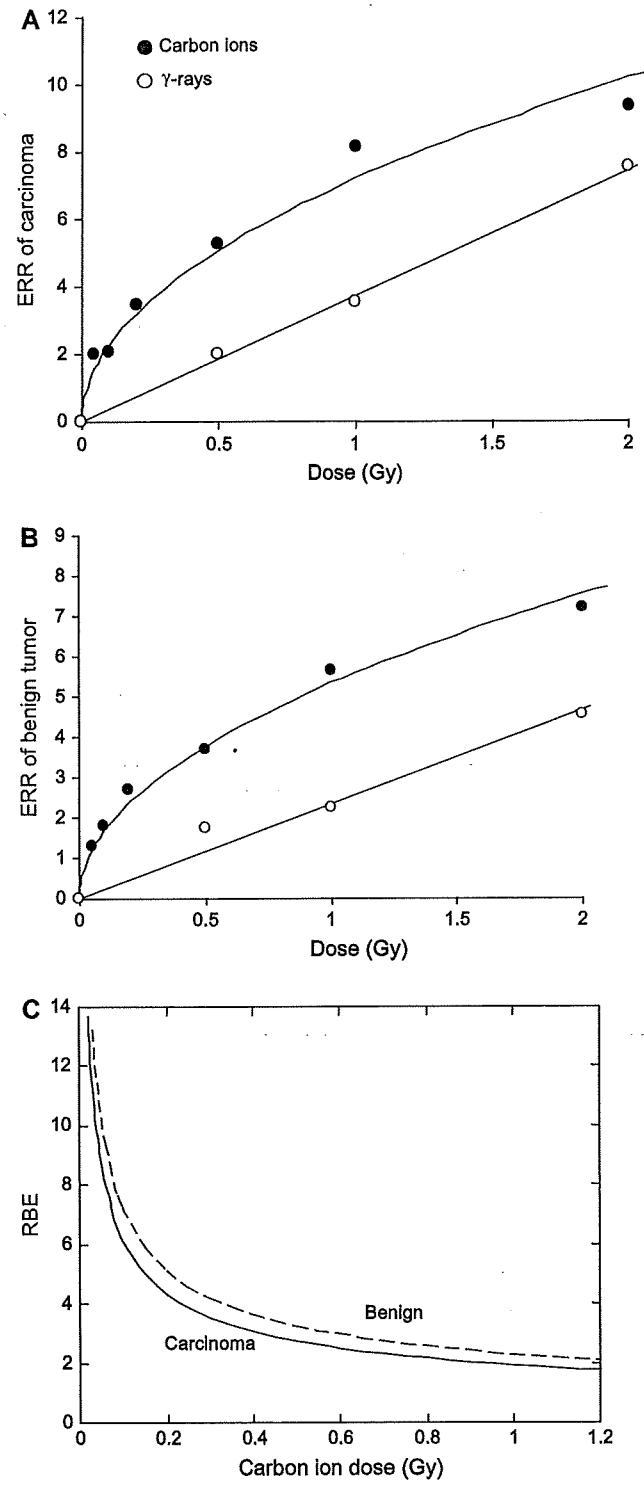

Fig. 4. Relative biologic effectiveness (RBE) for rat mammary tumor induction by carbon ions. Maximum likelihood method used to evaluate excess relative risk (ERR) for incidence of (A) carcinoma and (B) benign tumors. Carbon ion (black circles) data fitted using dose–square relationships and γ-ray (white circles) data fitted using linear relationships. (C) RBE for induction of carcinoma (solid line) and benign tumors (dashed line) expressed as functions of carbon ion dose.

H-*ras* codon 12 is a mutational hotspot in 1-methyl-1-nitrosourea-induced rat mammary carcinomas (16, 25). Hence, we examined 26 carcinomas (3 from ACI, 19 from

Table 5. Summary of results on relative biologic effectiveness of mammary carcinoma induction by high-LET radiation in rats of various strains

Strain	Radiation	Energy	Dose (Gy)	RBE	Reference
Present study					
Sprague-Dawley	C ion	290 MeV	0.05	8.6 ± 0.4*	
			1	1.9 ± 0.1*	
Published data					
Sprague-Dawley	Ne ion	6.6 GeV	0.02	>5	10
Sprague-Dawley	Fe ion	1 GeV	0.05–0.16	<10	11
Sprague-Dawley	Fast neutron	430 keV	0.064	13	7
ACI	Fast neutron	430 keV	0.045–0.36	10–15	8
Wistar WAG/Rij	Fast neutron	0.5 MeV	0.05–0.2	9–14	15
Brown Norway	Fast neutron	0.5 MeV	0.05–0.2	7–12	15
Sprague-Dawley (Dutch colony)	Fast neutron	0.5 MeV	0.05–0.2	5	15

Abbreviations: LET = linear energy transfer; RBE = relative biologic effectiveness.
* Data presented as mean ± standard error.

Sprague-Dawley, and 4 from Wistar rats) for this particular H-*ras* mutation using restriction fragment length polymorphism. These carcinomas completely lacked the mutation (data not shown). We also analyzed 13 Sprague-Dawley rat mammary carcinomas for common mutations in the tumor suppressor gene *Tp53*. We did not detect any new or commonly observed *Tp53* mutations by PCR or direct sequencing of genomic DNA sequences corresponding to exons 5–7 (data not shown).

DISCUSSION

The present therapeutic carbon ion study found that the Sprague-Dawley rat is susceptible to mammary carcinogenesis in contrast to the Wistar, F344, and ACI rats. The dose–effect relationship for the Sprague-Dawley rats was concave downward, with a significant increase in the carcinoma multiplicity at 0.05 Gy. The RBE for carcinoma incidence was inversely proportional to the square root of the dose. These carcinomas were mostly positive for ERα but negative for common H-*ras* and *Tp53* mutations. Lung metastasis of mammary carcinoma was unique to carbon ion–irradiated rats.

The aim of our study was to determine the RBE values *(1)* for risk estimation of therapeutic doses and *(2)* for the purpose of radiation protection against low-dose exposure. It is difficult to determine a single RBE value when the dose response of either the radiation under study or the reference radiation is nonlinear. An RBE value of 2, given by a typical dose per fraction (*i.e.*, ~1 Gy) (3), could be adopted for risk estimation of therapeutic doses. The maximal RBE (a limiting value of RBE at dose 0) can be the choice for use in radiation protection; however, the RBE approached infinity at dose 0 in the present study. Because the RBE value was 8.6 ± 0.4 at the smallest dose examined (0.05 Gy), we concluded that an RBE of ~10 should be considered in radiation protection. Strictly speaking, the characteristic occurrence of lung metastasis in our carbon ion–irradiated groups makes the application of RBE difficult because the idea of RBE is valid only if the effects of two radiations are qualitatively equal (26).

Several studies have focused on the carcinogenicity of heavy ions. In a series of studies on the mouse Harderian gland tumor, the RBE increased with LET, reaching a maximum of 30–45 at 100–200 keV/μm and did not decrease substantially thereafter ≤650 keV/μm (27, 28). Together with the present results, these data indicate that heavy ions have a strong effect on solid tumor induction. Shellabarger and coworkers (7, 10) conducted experiments on rat mammary carcinogenesis and showed that the RBE is >5 for 6.6-GeV neon ions at ~0.02 Gy (LET = 33 keV/μm) and 13 for 430-keV fast neutrons at 0.064 Gy (LET = ~70 keV/μm). Dicello *et al.* (11) reported that the RBE is <10 for 1-GeV iron ions at 0.05–0.16 Gy (LET = 155 keV/μm). As summarized in Table 5, previous studies on mammary carcinoma RBE have revealed that the fluctuation between strains is small. For safety, the RBE of susceptible strains should be adopted because the RBE is relatively low in resistant strains (15). Given the dose dependence found in our study, our estimation of the carbon ion RBE (LET = 40–90 keV/μm) is consistent with that of these reports.

In our carbon ion results, we noted a couple of characteristics in the shape of the dose–effect relationship such as downward concavity and a small peak at 0.05 Gy. In accordance with these findings, a concave downward relationship between dose and tumor incidence has been reported for high-LET radiation exposure in both humans and laboratory animals (7, 28, 29). Similar small peaks have also been observed in neutron-induced lung and mammary carcinogenesis (BALB/c mice) (30), as well as in heavy-ion–induced Harderian gland (B6CF1 mice), mammary and skin (Sprague-Dawley rats) tumorigenesis (10, 27, 31). The sublinearity and irregularity of the dose–effect relationship suggest a need to reconsider the validity of linear extrapolation for estimating the cancer risk at lower radiation doses, especially when considering the use in radiotherapy. As such, the recent development of precise heavy-ion irradiation devices such as a respiration-gated system (32) might contribute to reducing the risk of secondary cancers.

In the present study, the specific genetic status (rat strains) influenced the carbon ion effect on cancer induction.

Typically, the cell killing effect of heavy ions is not largely influenced by the genetic status of DNA repair machineries (such as *Tp53* mutations and non–homologous end joining defects) of the cells compared with the effects of low-LET radiation (33, 34). Thus, the different susceptibility to carcinomas among the different strains in the present study might not be attributable to differences in their DNA repair capabilities. This theory is further supported in that a variety of carcinogens (genotoxic chemicals and low- and high-LET radiation) exhibit identical strain dependence but produce a wide range of DNA damage (8–10, 12–14, 35–37). These include most DNA damage repaired by damage-specific mechanisms, as well as the damage produced by high-LET radiation, known as clustered damage, which is considered irreparable (38). Similarly, cellular radiosensitivity has correlated well between low- and high-LET radiation results, unless related to repair machinery defects (39). Although the exact nature of the particular strain difference exhibited in our study remains unclear, we did find a clear preference for tumor formation in Sprague-Dawley rats.

Ionizing radiation, especially with high LET, can induce genetic instability, which often results in selection of point mutations in cancer-related genes (40). Indeed, *Tp53* point mutations in α-emitter (Thorotrast)–induced human liver tumors are considered a secondary outcome of radiation-induced genetic instability (40). *Tp53* mutations are also found in many other radiation-associated human sarcomas (41, 42). Conversely, *Tp53* mutations have not been described in any cancers examined in the rat model system (43–48). Similarly, we did not find common *Tp53* mutations within exons 5–7 in the rat mammary carcinomas examined in this study. In addition to *Tp53*, H-*ras* mutations might be another marker for genetic instability. The H-*ras* gene often has point mutations in rat mammary carcinomas induced by chemical carcinogens (20, 25, 49). In contrast, we have previously revealed that radiation-induced rat mammary cancers have an intact H-*ras* gene (16). In agreement with this, we did not find mutations in the H-*ras* codon 12 in rat mammary carcinomas. Thus, heavy-ion–induced carcinogenesis does not appear to involve *Tp53* or H-*ras* mutations.

CONCLUSION

Therapeutic carbon ion radiation induced rat mammary carcinomas in a strain- and dose-dependent manner. An RBE value of 2 is appropriate for the risk estimation of therapeutic doses, and a value $\sim$10 should be considered for radiation protection of low doses. Examination of the carcinomas revealed that neither *Tp53* nor H-*ras* had mutated. These results have potential implications for ongoing thoracic heavy-ion radiotherapy, suggesting that genetically susceptible patients could be at greater risk of developing secondary breast cancers.

REFERENCES

1. Hirao Y, Ogawa H, Yamada S, *et al.* Heavy ion synchrotron for medical use—HIMAC project at NIRS-Japan. *Nucl Phys A* 1992;538:541c–550c.
2. Kanai T, Furusawa Y, Fukutsu K, *et al.* Irradiation of mixed beam and design of spread-out Bragg peak for heavy-ion radiotherapy. *Radiat Res* 1997;147:78–85.
3. Tsujii H, Mizoe JE, Kamada T, *et al.* Overview of clinical experiences on carbon ion radiotherapy at NIRS. *Radiother Oncol* 2004;73(Suppl. 2):S41–S49.
4. Ronckers CM, Erdmann CA, Land CE. Radiation and breast cancer: A review of current evidence. *Breast Cancer Res* 2004;7:21–32.
5. Preston DL, Mattsson A, Holmberg E, *et al.* Radiation effects on breast cancer risk: A pooled analysis of eight cohorts. *Radiat Res* 2002;158:220–235.
6. Land CE, Tokunaga M, Koyama K, *et al.* Incidence of female breast cancer among atomic bomb survivors, Hiroshima and Nagasaki, 1950–1990. *Radiat Res* 2003;160:707–717.
7. Shellabarger CJ, Chmelevsky D, Kellerer AM. Induction of mammary neoplasms in the Sprague-Dawley rat by 430keV neutrons and X-rays. *J Natl Cancer Inst* 1980;64:821–833.
8. Shellabarger CJ, Chmelevsky D, Kellerer AM, *et al.* Induction of mammary neoplasms in the ACI rat by 430-keV neutrons, X-rays, and diethylstilbestrol. *J Natl Cancer Inst* 1982;69:1135–1146.
9. Shellabarger CJ, Stone JP, Holtzman S. Rat differences in mammary tumor induction with estrogen and neutron radiation. *J Natl Cancer Inst* 1978;61:1505–1508.
10. Shellabarger CJ, Baum JW, Holtzman S, *et al.* Neon-20 ion- and X-ray-induced mammary carcinogenesis in female rats. *Ann NY Acad Sci* 1985;459:239–244.
11. Dicello JF, Christian A, Cucinotta FA, *et al.* In vivo mammary tumourigenesis in the Sprague-Dawley rat and microdosimetric correlates. *Phys Med Biol* 2004;49:3817–3830.
12. Vogel HHJ, Turner JE. Genetic component in rat mammary carcinogenesis. *Radiat Res* 1982;89:264–273.
13. Isaacs JT. Genetic control of resistance to chemically induced mammary adenocarcinogenesis in the rat. *Cancer Res* 1986; 46:3958–3963.
14. Moore CJ, Bachhuber AJ, Gould MN. Relationship of mammary tumor susceptibility, mammary cell-mediated mutagenesis, and metabolism of polycyclic aromatic hydrocarbons in four types of rats. *J Natl Cancer Inst* 1983;70:777–784.
15. Broerse JJ, Hennen LA, van Zwieten MJ, *et al.* Mammary carcinogenesis in different rat strains after single and fractionated irradiations. In: Broerse JJ, Gerber GB, editors. Neutron carcinogenesis. Luxembourg: Commission of the European Communities; 1982. p. 155–168.
16. Imaoka T, Nishimura M, Teramoto A, *et al.* Cooperative induction of rat mammary cancer by radiation and 1-methyl-1-nitrosourea via the oncogenic pathways involving c-Myc activation and H-*ras* mutation. *Int J Cancer* 2005;115:187–193.
17. Mohr U. International classification of rodent tumours. Part I: The rat. 5. Integumentary systems. Vol 122. Lyon: Oxford University Press; 1993.
18. Knott KK, McGinley JN, Lubet RA, *et al.* Effect of the aromatase inhibitor vorozole on estrogen and progesterone receptor content of rat mammary carcinomas induced by 1-methyl-1-nitrosourea. *Breast Cancer Res Treat* 2001;70:171–183.
19. Qiu C, Shan L, Yu M, *et al.* Steroid hormone receptor expression and proliferation in rat mammary gland carcinomas induced by 2-amino-1-methyl-6-phenylimidazo[4,5-*b*]pyridine. *Carcinogenesis* 2005;26:763–769.
20. Roberts-Thomson SJ, Snyderwine EG. Effect of dietary fat on codon 12 and 13 Ha-*ras* gene mutations in 2-amino-1-methyl-6-phenylimidazo[4,5-*b*]pyridine-induced rat mammary gland tumors. *Mol Carcinog* 1997;20:348–354.